University of Iowa

Iowa Research Online

Theses and Dissertations

Summer 2012

Graphene synthesis and characterization on copper

Ali Mohsin
University of Iowa

GRAPHENE SYNTHESIS AND CHARACTERIZATION ON COPPER

by

Ali Mohsin

A thesis submitted in partial fulfillment of the
requirements for the Master of Science degree
in Electrical and Computer Engineering
in the Graduate College of
The University of Iowa

July 2012

Thesis Supervisor: Assistant Professor Hassan Raza

Graduate College
The University of Iowa
Iowa City, Iowa

CERTIFICATE OF APPROVAL

_____

MASTER'S THESIS

_____

This is to certify that the Master's thesis of

Ali Mohsin

has been approved by the Examining Committee
for the thesis requirement for the Master of
Science degree in Electrical and Computer
Engineering at the July 2012 graduation.

Thesis Committee: _____
                     Hassan Raza, Thesis Supervisor

                     _____
                     David R. Andersen

                     _____
                     Markus Wohlgenannt

To my loving family.

ACKNOWLEDGMENTS

I am deeply thankful to my advisor, Prof. Hassan Raza for introducing me to the exciting area of graphene and giving me an opportunity to do experimental research in his lab. His expertise in the device research and experimental nanoscience has added a lot to my academic experience. I am especially thankful to him not only for his constant support and encouragement but also for his critical comments and pointing out the fine details that had important influence on my overall research experience.

I would like to thank Prof. David R. Andersen and Prof. Markus Wohlgenannt for serving on my thesis defense committee. I also thank Dr. Jonas Baltrusaitis for training me on the Almega Dispersive Raman microscope used in this study and also the Central Microscopy facility at the University of Iowa for allowing me to perform Raman study on the graphene samples. I am also thankful to Prof. Chris Coretsopoulos for training me on some of the equipment in the micro fabrication facility. I would like to thank Dr. Jonathon Olesberg for useful discussions and suggestions about operating some of the equipment in the micro fabrication facility. I also acknowledge Dr. Tehseen Raza for reading this thesis and giving her useful suggestions. I thank my colleague Ahmad Umair for his assistance during the lab work as well as useful discussions. Lastly, I thank my family for their constant support and encouragement.

ABSTRACT

Graphene, two dimensional sheet of carbon atoms has recently gained attention as some of its properties are promising for electronics applications e.g. higher mobility that translates to higher operating frequency for devices geared towards radio frequency applications. Excellent optical transmittance combined with its semi metallic behavior makes it an important material for transparent contacts in solar cells. To bring graphene to the production level, synthesis methods are needed for its growth on wafer scale. It has been shown that chemical vapor deposition (CVD) is one of the techniques that can potentially synthesize wafer scale graphene. Recently copper has gained popularity as an important substrate material for graphene growth due to its lower carbon solubility, which allows better control over number of graphene layers. Here we report optimization of graphene growth on copper foils with our home made atmospheric pressure chemical vapor deposition (APCVD) setup. Graphene growth on copper under APCVD was non self-limiting similar to earlier reports. It was found that apart from growth parameters surface texture plays a very important role in graphene growth. In fact, few layer and bilayer graphene were obtained on the regions where copper surface was not uniform, confirmed by Raman spectroscopy. To improve copper surface texture, thin layer of copper film was evaporated by electron beam evaporation before the graphene growth process. After this modification, monolayer graphene was obtained on areas as large as $300\ \mu m \times 300\ \mu m$, confirmed by Raman area maps. Graphene transfer procedure was also optimized so that graphene on metal surface could be transferred to insulating substrate.

TABLE OF CONTENTS

LIST OF TABLES

Table

LIST OF FIGURES

Figure

CHAPTER I

GRAPHENE

Introduction

The revolution in the electronics industry has been brought about by the miniaturization of the Integrated Circuits (IC) which serves as the key component of every electronic device. This has been made possible by the continued scaling in the dimensions of the field effect transistor (FET) which is the workhorse of IC [1]. The typical size of FET has reached nanoscale regime where short channel effects starts dominating which hinders its further scaling [2]. Silicon is currently used as channel material for FET, but currently new materials are actively studied that can replace silicon in the future nanoscale FET`s. Graphene is one of those materials which are topic of current research interest due to its excellent properties e.g. one atom thick [3], mobility of the order of *200000 cm^2/Vs* [4,5], ability to with stand current density of *10^8 A/cm^2* [6], transmittance of about *97%* of visible light [7] and high thermal conductivity of the order of *5 × 10^3 W/mK* [8]. It was long believed that two-dimensional materials (2D) were unstable thermodynamically and they only serve as building blocks of complex three dimensional (3D) structures [3]. However, experimental evidence of 2D crystals came in 2004 [4] and 2005 [9] when thin flakes of graphene and other materials molybdenum disulphide, niobium diselenide and hexagonal boron nitride were first exfoliated from their bulk counterparts. Graphene is the name given to arrangement of carbon atoms on hexagonal honeycomb lattice that is exactly one atom thick [10]. It is this arrangement and symmetry of carbon atoms that gives unique properties to graphene [11]. Graphene was first obtained in the form of small flakes of the order of several microns through mechanical exfoliation of graphite using scotch tape [4,9]. Though this method gives the highest quality graphene but to bring graphene to the production scale, fabrication

method is needed that can synthesize wafer scale graphene. Chemical vapor deposition (CVD) is one technique that has the ability to synthesize wafer scale graphene [12]. The method mainly involves the adsorption, decomposition and segregation of carbon containing precursor on the transition metal surface at elevated temperature either at low or atmospheric pressure which results in graphene synthesis. The aim of this project is to synthesize monolayer graphene through CVD method. Growth parameters are optimized for our home made atmospheric pressure chemical vapor deposition system. In this study, copper had been used as the substrate material for graphene synthesis due to its small carbon solubility at elevated temperatures [13] which allows better control over the number of graphene layers. Transfer method is also optimized so that synthesized graphene on metal surface can be transferred to insulating substrates for fabricating devices.

The thesis is organized as follows. Chapter 1 is devoted to the discussion of graphene band structure responsible for its excellent electronic properties, various methods for graphene production including CVD and techniques for graphene transfer to insulating substrates. Chapter 2 describes graphene synthesis process flow starting from copper substrate to its transfer onto SiO_2/Si. We discuss experimental observations and results in Chapter 3. The summary of this experimental study and future work are presented in Chapter 4.

<u>Graphene band structure</u>

Each carbon atom in graphene undergoes sp^2 hybridization between one *2s* and two *2p* oribtals resulting in three sp^2 hybridized orbitals. Each carbon atom on honeycomb lattice forms three sigma (σ) bonds with three in plane nearest neighboring carbon atoms. The remaining *2p* orbitals on each carbon atoms, which are perpendicular

to planar structure form pi (π) bonds which are half filled [14]. σ-bonds in all allotropes of carbon including graphene are responsible for the mechanical strength [15].

In order to derive band structure of graphene under tight binding approximation, consider honey comb lattice of graphene as shown in Fig. 1(a). The basic unit cell identified in rectangle consists of two in equivalent carbon atoms 1 and 2. Real space lattice vectors in this case are:

$$\boldsymbol{a_1} = \frac{a}{2}(3, \sqrt{3}), \quad \boldsymbol{a_2} = \frac{a}{2}(3, -\sqrt{3})$$

where $a = 1.42\text{Å}$ is the carbon-carbon bond length.
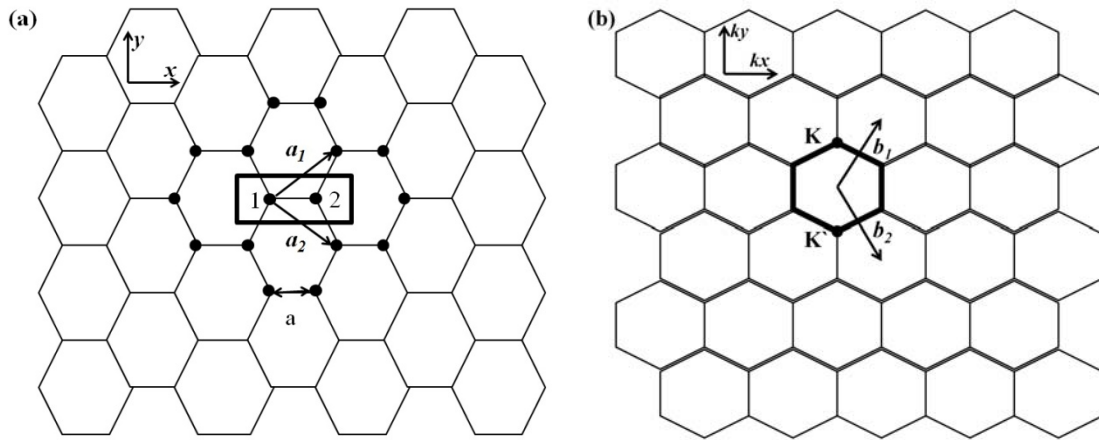
Figure 1. Hexagonal honey comb lattice of graphene. (a) Real space lattice. (b) Reciprocal space lattice.

Reciprocal space lattice vectors are:

$$\boldsymbol{b_1} = \frac{2\pi}{3a}(1, \sqrt{3}), \quad \boldsymbol{b_2} = \frac{2\pi}{3a}(1, -\sqrt{3})$$

The corresponding reciprocal space lattice is shown in Fig. 1(b) which shows that first Brillouin zone for graphene is also hexagonal. Band structure of a periodic solid

is given by determinant of following equation [16].

$$[E\boldsymbol{I} - h(\boldsymbol{k})]\{\boldsymbol{\Phi_o}\}= 0 \tag{2.1}$$

Where $h(\boldsymbol{k}) = \sum_m [H_{nm}]e^{i\boldsymbol{k}\cdot(\boldsymbol{d_n}-\boldsymbol{d_m})}$ and I is the identity matrix

Index n is for nth unit cell and the summation runs over all m neighboring unit cells. H_{nn} is the onsite energy and H_{nm} is the overlap integral. For the case of nth unit cell, assuming nearest neighbors only with zero onsite energy ($H_{nn} = 0$), $h(\boldsymbol{k})$ is given by:

$$h(\boldsymbol{k})=\begin{bmatrix} 0 & h_o \\ h_o^* & 0 \end{bmatrix} \tag{2.2}$$

where $h_o = -t\left(1 + e^{ik\cdot a_1} + e^{ik\cdot a_2}\right) = -t\left(1 + 2e^{i\frac{3ak_x}{2}}cos\frac{\sqrt{3a}k_y}{2}\right)$

and $H_{n,n\pm1} = -t$ is the tight binding parameter. With $h(\boldsymbol{k})$ given in Eq. 2.2, the eigen values of matrix given in Eq. (2.1) are $\pm|h_O|$ and they are plotted in Fig. 2.

The importance of this band structure is that two set of bands meet at six reciprocal space basis vectors points (k_x,k_y) i.e $(0,-4\pi/3\sqrt{3}a)$, $(2\pi/3a,-2\pi/3\sqrt{3}a)$, $(2\pi/3a,2\pi/3\sqrt{3}a)$, $(0,-4\pi/3\sqrt{3}a)$, $(-2\pi/3a,2\pi/3\sqrt{3}a)$, $(-2\pi/3a,-2\pi/3\sqrt{3}a)$. Each of these corner points are shared by 1/3rd of the corresponding Brillouin zone and hence there are essentially two Valley points K and K' as identified in Fig. 1(b) where the band gap is zero.
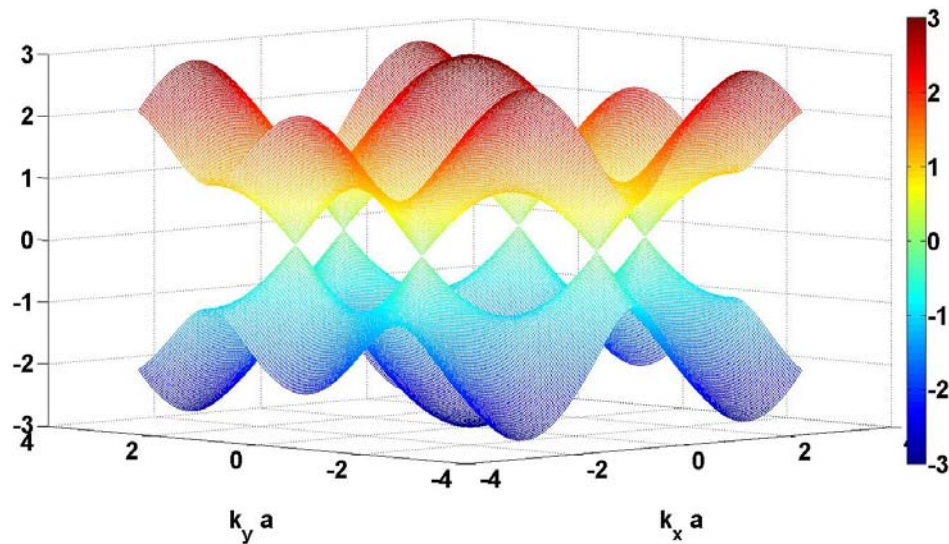
Figure 2. Graphene band structure [16].

Graphene synthesis methods

We discuss the following methods for graphene synthesis in this section.

Mechanical exfoliation

Graphene was first obtained from bulk highly ordered pyrolytic graphite (HOPG) by mechanical exfoliation (repeated peeling) using scotch tape [3,4,9]. Layers in bulk graphite are held together by weak van der Waals energy of the order of $2\ eV/nm^2$ and the force of about $300\ nN/\mu m^2$ is required to remove monolayer graphene from graphite [17]. Such small force can easily be managed by adhesive tape. After repeated peeling, graphene from adhesive tape can be transferred to SiO_2/Si substrate by gentle pressing [4,9]. To distinguish between layers of graphene, the thickness of SiO_2 is important because at the thickness of $90\ nm$ or $280\ nm$, graphene contrast on SiO_2 is maximized by about 12% at $550\ nm$ where the sensitivity of human eye is optimal [18]. Fig. 3 shows optical image of graphene transferred by mechanical exfoliation onto $\sim 300\ nm$ SiO_2.

yellow regions in Fig. 3(a) represents thin graphite layers of the order of *100 nm* and light purple region in Fig. 3(a) and Fig. 3(b) shows monolayer graphene [19]. Graphene obtained by this method has shown properties close to theoretical predictions e.g. mobility of the order of 10^6 *cm^2/Vs* [20,21]. The problem with this method is that it
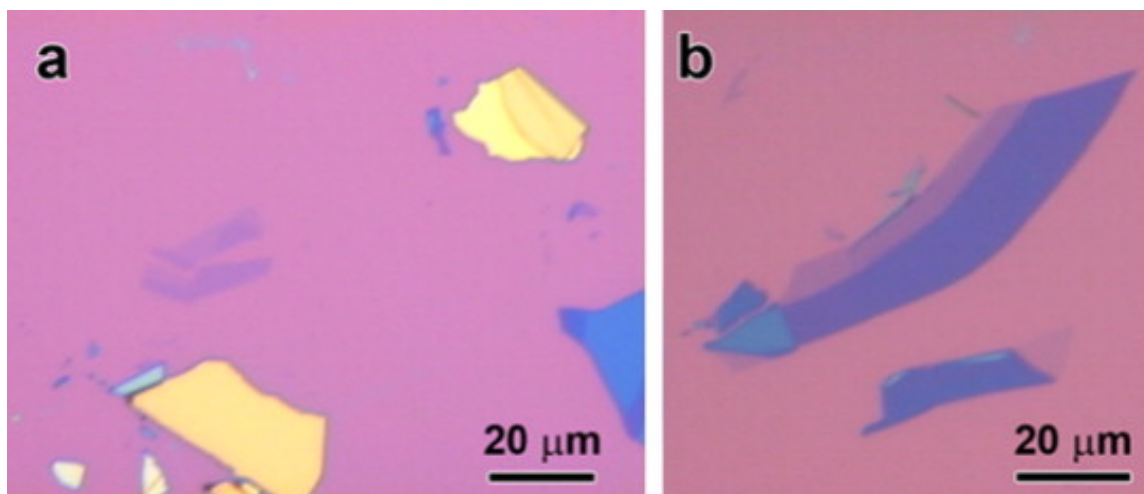
Figure 3.   Micromechanically exfoliated graphene. Optical images of (a) thin layer graphite and (b) Few layer graphene (FLG) and single layer graphene (light purple contrast) on ~ *300 nm* SiO$_2$ [19].

leaves residues of adhesive tape that can result in mobility degradation [22,23]. To partially remove contamination, heat treatment under Ar/H$_2$ atmosphere at $200^\circ C$ [24] or *in situ* Joule heating by the application of current of the order of *micro amperes* may be used [6]. The size of graphene flakes obtained by this method is limited and this is the key issue towards large scale graphene synthesis by this method. But still this method remains benchmark to compare electronic properties of graphene obtained by other techniques.

Graphitization of silicon carbide

Silicon Carbide (SiC), a highly resistive material when heated around $1400^\circ C$ under vacuum results in sublimation of silicon with the result that graphitization of remaining carbon takes place [25]. The problem with high temperature vacuum annealing of SiC is that it results in highly corrugated surface covered by small graphene regions with varying thickness [26]. One solution to this problem was to use *C terminated SiC* instead of previously used *Si terminated SiC* that resulted in improved graphene coverage of the order of *1 μm* [27]. However much higher graphene coverage with this method was achieved by graphitization near atmospheric pressure under Ar ambient that resulted in smooth surface with graphene coverage as large as *50 μm* [28]. The reason for this improved coverage was the reduced sublimation of silicon atoms due to higher temperature around $1650^\circ C$ under Ar ambient at near atmospheric pressure [26,28]. The graphene obtained by this method showed field effect mobility only five times smaller than exfoliated graphene [28]. The problem with this technique is that the initial cost of the SiC wafer is high and also it requires very high temperature around $1400\text{-}1600^\circ$C.

Wet chemical route

The basic idea behind this technique is to intercalate layers of graphite derivates with different reactants that results in the separation of these layers from the bulk. The precursor is usually graphite which is first reacted with strong acids and oxidants to produce graphite oxide [29]. As a result of this reaction, various hydroxyl and epoxide groups attach to the carbon atoms in graphite oxide through covalent bonds [30,31] with the result that though original layered structure of graphite is retained but conjugated structure of carbon atoms is severely distorted [29]. Graphite oxide is thus layered

structure of graphene oxide sheets that do not preserve the original conjugated bond structure of graphite [32]. An attempt to reduce graphene oxide with various reducing agents e.g. *hydrazine, dimethylhydrazine* and *hydroquinone* result in colloidal suspension of varying conductivity and graphene flakes of different lateral sizes and thickness [29]. The challenge in this approach is that original structure of graphite is modified and even after treatment with reducing agents, the original sp^2 network of carbon atoms in not restored. To overcome this problem, non covalent functionalization of conjugated carbon network in graphite is achieved through *1-pyrene carboxylic acid* [33] and *9-anthracene carboxylic acid* [34]. The advantage of this scheme is that external functional groups attach to carbon network through π-π stacking rather covalent bond formation. As a result of π-π stacking, the conjugated network of sp^2 bonded carbon atoms in graphite is retained and the obtained graphene flakes shows improved electrical properties [34]. Though non covalent functionalization improves electrical properties of resulting graphene flakes, the scalability of this method to wafer scale is still challenging. This method in general can be refined to obtained graphene nanoribbons (GNR) which are one dimensional analogue of graphene. One approach in this direction is the chemical unzipping of carbon nanotubes [35] but again most important properties of GNR`s are contained in specific edge orientation [36-38] and much efforts are needed in this direction to obtain GNR with precise edges.

Chemical vapor deposition

The essence of this technique is that precursors in the vapor phase adsorb and react at the substrate surface at elevated temperatures under low pressure (of the order of *milli torr*) or atmospheric pressure that results in the deposition of thin film as a result of chemical reaction. In case of graphene synthesis, precursors are usually carbon containing gas e.g. methane or vapors of any liquid carbon source e.g. alcohols that react on the transition metal surface under the ambient environment (e.g. Ar to avoid

deposition of amorphous carbon). It is well known that transition metals serve as efficient catalysts in transforming hydrocarbons into graphitic materials [19] and graphite layers were obtained on Nickel surface from either hydrocarbons or evaporated carbon in early 1960's [39]. Graphene obtained recently [40,41] is the result of refinement of previous methods to get controllable deposition. The solubility of carbon in transition metal along with CVD conditions play an important role in determining growth mechanism and ultimately controls the number of graphene layers [39]. Recent promising results of graphene growth on copper shows that it may serve as alternate route towards scalable growth of graphene with higher monolayer coverage [42,43]. The solubility of carbon in copper is negligible of the order of ppm even at $1000^{\circ}C$ [11] so the carbon precursor forms graphene directly on copper surface during growth step [44].
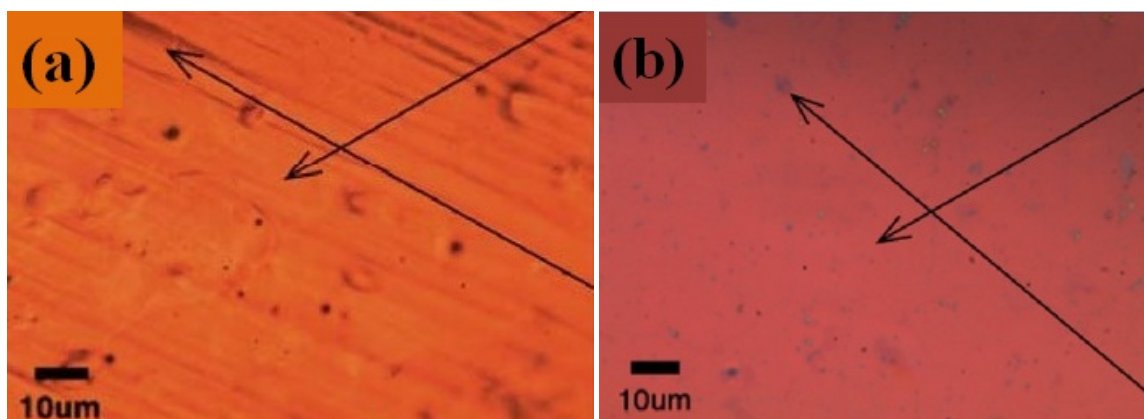
Figure 4.   CVD grown graphene on copper. Optical images of (a) as-grown graphene and (b) transferred to *300 nm* SiO$_2$. Black arrows in(a) shows corrugations on copper surface that results in multilayer graphene highlighted by black arrows close to purple regions in (b) [45].

Commercial copper foils have been used for the graphene synthesis to reduce overall cost of fabrication process but these foils have strongly corrugated surface due to cold rolling process during manufacture and this surface roughness is known to produce

graphene thickness variation on copper [46,47]. Since graphene growth on copper is surface limited, so smoothness of copper surface plays very important role in getting monolayer coverage across the entire surface of the substrate [48]. Fig. 4(a) shows optical image of as grown graphene on copper, the corrugations on metal foil are highlighted by black arrows. Fig. 4(b) shows same graphene when transferred to *300 nm* SiO$_2$. Here dark purple regions highlighted by black arrows shows that even on low carbon solubility metal like copper, corrugations on starting substrate can result in formation of significant multilayer regions along with monolayer graphene [45]. From electronic applications point of view, field effect mobility, transmittance and sheet resistance are the important parameters. For CVD grown graphene shows field effect nobilities of the order of *3000 cm^2/Vs* [39], optical transmittance of the order of *90%* [49] and sheet resistance of the order *280 Ω/sq* [40]. It must be mentioned that graphene obtained by CVD is inferior to graphene obtained by mechanical exfoliation in terms of above mentioned parameters. One reason is that graphene obtained by CVD is in the form of continuous sheet which is inherently polycrystalline because graphene domains of different orientations merge together to from graphene sheet and because of the presence of grain boundaries, the overall film shows poor electrical properties [50-52]. So efforts have begun in this direction to obtain single crystal isolated graphene domains with improved electrical properties [53-55]. Another major problem with CVD is that graphene is obtained on top of metal surface but for electronic devices applications, it needs to be transferred to insulating substrates e.g. SiO$_2$. During the transfer process, unavoidable structural damage occurs to graphene [56,57] which can degrade its electronic electrical properties. Further efforts in this direction are required to obtain transfer free single crystal graphene.

Annealing solid carbon sources

In this method similar to CVD, the substrate is heated to elevated temperature under ambient environment but there is an important difference that actual carbon

precursor in this case is in the form of solid which is usually evaporated or spin coated on metal surface. Graphene has been obtained through various precursors using this method including Polymethylmetacrylate(PMMA) [58], amorphous carbon [59] on copper surface and Polyacrylonitrile(PAN), Polystyrene(PS), PMMA [60,61], C_{60} [62] on nickel surface. A variant of this method has also been demonstrated in which carbon source is first deposited on SiO_2/Si and then metal thin film is evaporated and annealed at elevated temperatures. The advantage of this variant is that graphene need not to be transferred to other insulating substrate. This has been demonstrated for the case of C_{60} [62] and self assembled monolayer (SAM) [63] on nickel thin film evaporated on SiO_2/Si. The graphene obtained by this method shows field effect mobility comparable to CVD grown graphene [59]. Another advantage of this method is that *in situ* doped graphene can be obtained by using solid carbon precursor that also contains desired dopant element [63]. Till now, this method has same limitation as that of CVD i.e. obtained graphene is polycrystalline containing grain boundaries. However the variant of this technique in which carbon source is deposited below the metal film shows promise towards transfer free single crystal graphene but much research is needed in this direction. It is worth noting that this method is relatively new and the actual chemical kinetics that results in graphene formation are still the topic of active research.

Graphene transfer

The graphene on metal surface needs to be transferred to insulating substrate for device fabrication. After graphene growth, the top of metal is covered with "handle" which serve as mechanical support for underlying graphene film. This handle can be PDMS stamp, spin coated polymer e.g. PMMA, thermal release tape or scotch tape. After that, bottom transition metal substrate is etched using standard wet etchant. 1M $FeCl_3$ is normally used as etchant for copper as it etches slowly allowing better control of etch rate but more importantly, it does not generate gas bubbles like other etchants, which

can induce cracks in transferred graphene films [39,40]. After etching "handle/graphene" stack is transferred to de-ionized (DI) water bath for rinsing to remove residual etchant. The stack is then placed on target substrate and allowed to dry naturally. Now depending upon the material of handle, different techniques can be used to remove it. PDMS handle can be just peeled off leaving graphene film on target substrate. If the handle is PMMA or scotch tape, it can be removed by dissolving in acetone. PMMA leaves residues even after cleaning so additional annealing step at $450^{\circ}C$ under Ar and H_2 may be required [47]. With thermal release tape as handle, the target substrate is heated at the rated temperature on hot plate where the tape loses its adhesive strength. After removing tape, the tape residue can be dissolved in organic solvents e.g. acetone, methanol. If the underlying transition metal is in the form of thin film on some substrate e.g. copper thin film on SiO_2/Si, then additional step may be required to lift off "graphene/metal film" stack from the substrate (e.g. by dipping in HF or Buffered Oxide etch [40] if the film is on SiO_2/Si) before etching, otherwise etching will be too slow (if the etchant is $FeCl_3$) and more importantly it may leave etching residues between transferred graphene and underlying substrate after etching.

CHAPTER II

GRAPHENE SYNTHESIS AND TRANSFER

This Chapter gives details of all experimental methods involved in the graphene synthesis and transfer to insulating substrate. Fig. 5 summarizes these steps.
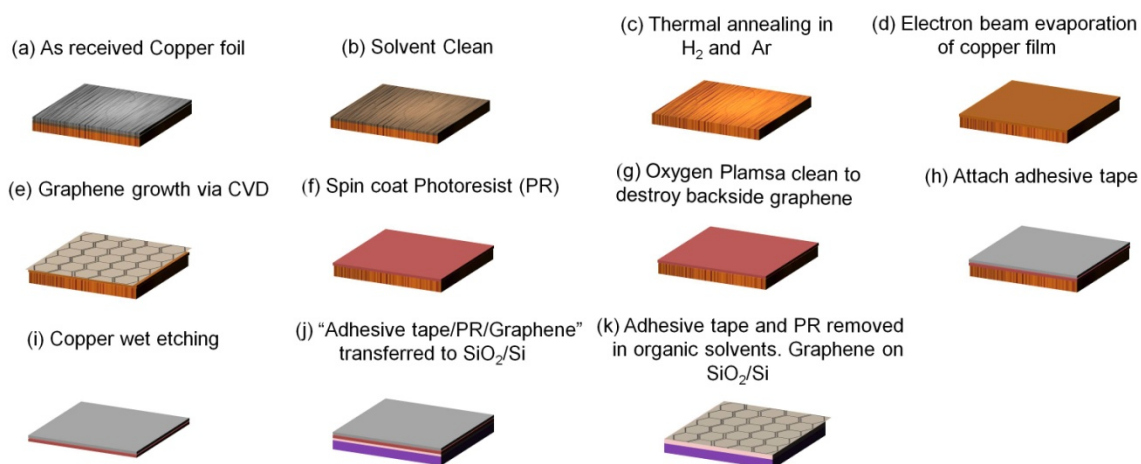
Figure 5.   Process flow for graphene synthesis and transfer to SiO_2/Si.

Solvent cleaning

The starting substrate is *25μm* thick, *99.999%* pure copper foil from Alfa Aesar (*Product No.10950*). The as-received copper foil may contain thin layer of grease or organic impurities that may result in the deposition of amorphous carbon at high temperatures [64], so solvent cleaning step is performed to remove them. The recipe for solvent cleaning step is summarized in Table 1. Acetone is used mainly to remove organic impurities but it also leaves its own residues due to its very fast evaporation rate so methanol is used as solvent to remove left over acetone [65]. Finally foil is placed in De-ionized (DI) water bath to remove remaining organic solvents. After Nitrogen dry

Table 1.   Solvent cleaning recipe.

Acetone	Methanol	De-ionized Water (DI) dip	Nitrogen dry	Ozone Clean
5 minutes	5 minutes	5 minutes	Gently until foil is dry	2 minutes

step, foil is pressed between two clean quartz slides to keep it as straight as possible. During ozone clean, foil is placed on clean quartz slide that is also used during thermal annealing step.

Thermal annealing

As received copper foil contains thin layer of native copper oxide, which is highly undesirable for graphene growth [39]. Acetic acid may be used to remove native oxide layer [66] but it leaves the surface too rough which is also not desirable [47]. Thermal annealing of annealing of copper foil is performed in Ar and H_2 at $900^{\circ}C$. The purpose of thermal annealing is two-fold: first, to remove native copper oxide layer by H_2 reduction [39,67] and second, to increase the grain size of polycrystalline copper foil. As received foil has much smaller grain size with large number of grain boundaries. Graphene tends to grow preferentially on grain boundaries first as compared to flat copper surface, which ultimately leads to multilayer graphene on those regions [48,55]. Thermal annealing increase copper grain size [39] which reduce the effect of grain boundaries on graphene growth.

Thermal annealing was performed in our home made CVD system. It essentially consists of Lindberg blue M furnace with *1 in*. diameter quartz tube. The tube can be fed by Ar, H_2 and CH_4. The flow rate of CH_4 and H_2 is maintained by single regulated flow meter while Ar flow rate is measured by unregulated flow meter. Typical thermal annealing recipe is summarized in Table 2. Copper foil on quartz slide was loaded into

the quartz tube and the temperature was ramped up to *900°C* under H_2 (*36 sccm**) and Ar (*280 sccm*) ambient. H_2 was used during the ramp up step to avoid oxidation of copper at elevated temperatures. After reaching the annealing temperature, flow rate of gases were left unchanged and annealing was performed for *2 hours*. After the annealing step, temperature was ramped down and furnace was allowed to cool down naturally under H_2 (*36 sccm*) and Ar (*280 sccm*) ambient. Copper foil was unloaded from the quartz tube at room temperature.

Table 2.   Thermal annealing recipe.

Step Number	Processing Step	Temperature	Processing gas	Duration (minutes)
1	Ramp up	900°C	Ar (280 sccm) and H_2 (36 sccm)	20
2	Annealing	900°C	Ar (280 sccm) and H_2 (36 sccm)	120
3	Ramp down	Room temperature	Ar (280 sccm) and H_2 (36 sccm)	Natural cool down

Electron beam evaporation

The electron beam evaporator used for copper thin film evaporation was AMOD 006 series system manufactured by Angstrom Engineering. After loading copper foils into the evaporation chamber, the chamber was evacuated. The evaporation process started when the pressure of the chamber reached below *1×10^{-6} torr*. The actual deposition is controlled by Sigma control software. To start evaporation, power in the

---

* sccm stands for standard cubic centimeters per minute

Sigma control software was increased at the rate of *0.1%* every *20 seconds*. This higher ramp rate was chosen because crucible for copper evaporation was Molybdenum which is metal and hence it can bear thermal stress. When the evaporation rate of copper reached *2 Å/s*, shutter was opened from the main control software and copper film began to deposit on the target substrate. When the desired thickness was reached, shutter was closed and power was decreased at *0.1%* every *20 seconds*. Sample was unloaded one hour after the completion of evaporation process to avoid oxidation of hot copper source. Typical evaporation parameters for copper are summarized in Table 3.

Table 3. Parameters for copper electron beam evaporation.

Crucible	Chamber pressure (torr)	Evaporation rate (Å/sec)	Acceleration Voltage (kV)	Source current (mA)	Copper density (gm/cm^3)	Copper Z factor
Molybdenum	9×10^{-7}	2	-8.16	180	8.92	0.437

<u>Chemical vapor depositon</u>

Graphene growth was performed in our home made atmospheric pressure hot wall chemical vapor deposition (APCVD) system. This is the same setup that was used for annealing of copper foils. Graphene growth recipe is summarized in Table 4. Copper foil with evaporated copper film was placed on quartz slide and loaded into the quartz tube of CVD furnace. The temperature was ramped up to *1000°C* under H_2 (*36 sccm*) and Ar (*280 sccm*) ambient. H_2 was used during the ramp up step to avoid oxidation of copper at elevated temperatures. After reaching the growth temperature , H_2 supply was closed and CH_4 (*5 sccm*) supply was opened. Growth process typically continued for *2 minutes* at *1000°C*. After the growth step, CH_4 was closed and sample was fast cooled by moving

the quartz tube out of the furnace. Sample was unloaded, *1 hour* after the fast cooling step.

Table 4.   CVD recipe for graphene growth.

Step Number	Processing step	Temperature	Processing gases	Duration (minutes)
1	Ramp up	1000°C	Ar (280 sccm) and H_2(36 sccm)	20
2	Growth	1000°C	Ar (280 sccm) and CH_4 (5 sccm)	2
3	Ramp down	Room temperature	Ar (280 sccm)	5†

<u>Graphene transfer</u>

After unloading samples from CVD furnace, "handle" of polymer film was deposited on foil to serve as mechanical support for graphene film during subsequent processing steps. *AZ 9260 Photoresist* (PR) was chosen as it can coat thick films upto *14µm* in single coat [68]. The advantage of PR is that it can be easily removed in solvents e.g. acetone as compared to commonly used polymer *Polymethylmethacrylate (PMMA)* which leaves residues even after the solvent cleaning step [47]. For depositing PR film, foil was placed on sample stage of homemade spin coater and PR was poured on the foil. After that, recipe in Table 5 was followed for spin coating. During CVD growth graphene grows on both sides of copper foil. The back side graphene is not desired and it can be removed by oxygen plasma clean [69]. Oxygen plasma clean was performed in plasma cleaner *PDC-32G* manufactured by Herrick Plasma. Table 6 summarizes conditions

---

† Samples are fast cooled to room temperature by moving tube quickly out of the furnace.

Table 5.   *AZ 9260* spin coating recipe.

Step Number	Processing step	Attribute	Duration (seconds)
1	Initial ramp	500 rpm	10
2	Spreading	1500 rpm	50
3	Soft bake	$120^{\circ}C$	300

during typical plasma clean. After loading sample into the plasma cleaner, chamber was evacuated. Then plasma was generated and oxygen supply was connected to the chamber. After the cleaning step, oxygen supply was closed and plasma was extinguished. The sample was unloaded after venting the chamber with ambient air.

Table 6.   Plasma cleaning conditions.

Plasma power	Oxygen flow rate	Duration
High (18W)	5sccm	16 minutes

After plasma cleaning step, an additional layer of scotch tape was attached on top of foil with spin coated PR film. This scotch tape layer served as an additional mechanical support. After attaching adhesive tape, foil was placed in 1M FeCl$_3$ bath. Typically for *25 μm* thick foil, copper etching took approximately *3 hours*. When the copper etching was complete, a pre-cleaned piece of *300nm* SiO$_2$ on silicon was taken and graphene membrane was scooped out from FeCl$_3$ onto SiO$_2$/Si and transferred to DI water bath. Meanwhile, SiO$_2$/Si piece was placed for DI rinse. Since graphene membrane is fragile it cannot be placed in DI rinse. DI dip was done for *10 minutes* to remove FeCl$_3$ residue. After DI dip, graphene membrane was again scooped out onto SiO$_2$/Si piece and dried very gently with Nitrogen. During this step, care may be taken that since residual

water may be present on substrate and during drying membrane may slip over water layer and can fall off the substrate. The substrate was then placed on hot plate preset at $50^{\circ}C$ for *15 minutes*. This step was done to evaporate thin layer of water that may be present on substrate. Then temperature was increased to $70^{\circ}C$ and the substrate was heated for another *15 minutes*. This was done to further evaporate remaining water between graphene and SiO_2 and also to improve the adhesion of graphene to the substrate [69]. After this step, substrate with attached graphene membrane was transferred to acetone bath for 10 minutes, to remove both adhesive tape and PR. The substrate was transferred to methanol bath for *10 minutes*, to remove left over acetone residue. Finally substrate was placed in DI rinse for *10 minutes* to remove left over organics. Subsequently, the substrate was dried with Nitrogen and the sample was ready for characterization.

CHAPTER III

RESULTS AND DISCUSSIONS

<u>Graphene characterization</u>

The objective of   graphene characterization is two-fold: first to identify number of layers in a given sample and second to determine the quality of grown film in terms of defects. Raman spectroscopy was used for the graphene characterization because Raman spectrum of graphene contains characteristic bands which can be used to distinguish among number of graphene layers and also gives information about defects in the sample [70]. Also it is fairly easy to generate spatial Raman area maps of the order of hundreds of microns to study spatial uniformity.

Raman spectrum of graphene

Phonons are quantum of lattice vibrations [71] and in order to identify Raman spectrum of graphene, it is important to identify first phonon dispersion of graphene. The unit cell of graphene as shown in Fig 1(a) contains two atoms and vibrations of these two atoms can be in phase which leads to *acoustic phonons* and out of phase which leads to *optical phonons*. For each of acoustic or optical phonon, vibration of each of these two atoms can be in carbon-carbon direction which leads to *in-plane longitudinal acoustic phonons (iLA)* and *in-plane longitudinal optic phonons (iLO)*. Similarly in plane vibrations perpendicular to the carbon-carbon direction leads to *in-plane transverse acoustic phonons (iTA)* and *in-plane transverse optic phonons (iTA)*. Vibrations of the atoms can also be perpendicular to the plane containing the carbon atoms which leads to *out-of-plane transverse optic phonons (oTA)* and *out-of-plane longitudinal optic phonons (oLA)*. Combining all these cases, there are six phonon dispersions for graphene as shown

in Fig. 6(a). The Raman spectrum of monolayer graphene derived from these phonon dispersions [72] is shown in Fig. 6(b). The important peaks in the spectrum and their
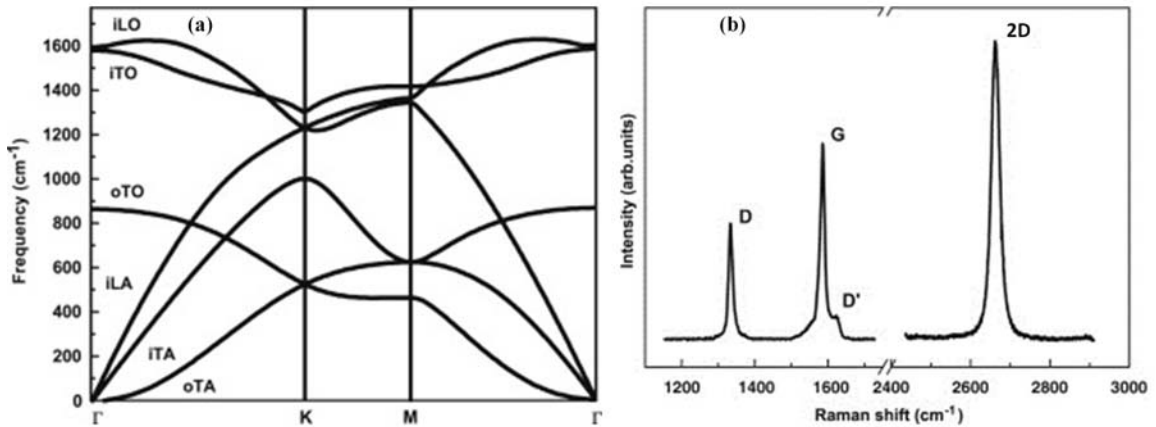
Figure 6.   Phonon dispersion and Raman spectrum of graphene (a*) iLO, iTO, oTO, iLA, iTA,oTA* phonon brances along high symmetry points *ΓM* and *ΓK* (b) *D, G, D′* and *2D* peaks in Raman spectrum [72].

origin is explained below.

The most prominent peaks in the Raman spectrum are *G* and *2D* bands occurring at about *1580 cm^{-1}* and *2700 cm^{-1}* respectively. The *G* band is due to two doubly degenerate phonon modes *iTO* and *iLO* [Fig. 6(a)] at the zone centre *(Γ point)*. *G* band occurs due to first order Raman scattering process involving only absorption and release of photon as shown in Fig. 7(d). The *D* band which occurs around *1350 cm^{-1}* is due to *Double resonance (DR) Raman scattering process* involving one *iTO* phonon and one crystal defect near the *K* point as shown in Fig. 7(a). For *D* peak, *DR* process as shown in Fig. 7(a) starts with an electron around valley point *K* which absorbs incident photon and gets elastically scattered by defect in crystal to another electronic state belonging to circle centered on valley point *K′*. The electron is then in-elastically scattered back to the

original state by electron-phonon interaction and finally release photon by combining with hole. This *DR* process include one elastic scattering event caused by defect of crystal and one inelastic scattering event induced by electron-phonon interaction. The *DR* process for *2D* peak is similar, with the only difference that both scattering events
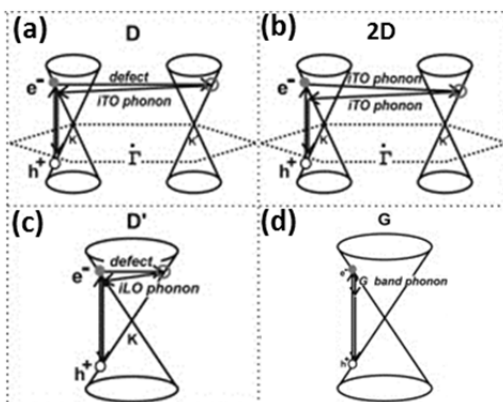
Figure 7.   Double Resonance Process for: (a) *D* peak, (b) *2D* peak and (c) *D′* peak. (d) Single Resonance process involved in G peak [72].

are in elastic induced by interaction of electron with two phonons of equal and opposite wave as shown in Fig. 7(b). It is interesting to note that name of *2D* peak comes from the fact that it occurs at approximately twice wave number than that of *D* peak but as explained above as it does not require any defect in crystal for its activation so this peak is always present even if *D* peak is negligible. There is another peak at approximately *1620 cm^{-1}* which is named as *D′* and it also arises because of *DR* process. But in this case electron is scattered to neighboring state on the same circle around *K* or *K′* valley point. *DR* process for *D′* requires one defect and one *iLO* phonon for activation as shown in Fig. 7(c).

<u>Results and discussions</u>

Atmospheric pressure chemical vapor deposition (APCVD) has been used for graphene growth in this study. The important parameters in APCVD include flow rate of precursor gas, temperature and growth time. CH_4 was used as precursor gas while H_2 and Ar were used as carrier gases. Copper foil was used as substrate for graphene growth. After performing solvent clean on copper substrate as mentioned in Chapter 3, recipe in Table 7 was followed for initial set of growth experiments. Temperature ramp up step was performed in H_2 and Ar ambient. H_2 was kept flowing to avoid oxidation of copper foil [45]. Thermal annealing was performed at elevated temperature to reduce native copper oxide by H_2 reduction as well as to increase copper grains before the growth step

Table 7.   Graphene growth recipe for initial set of experiments.

Step Number	Processing step	Temperature	Processing gases	Duration (minutes)
1	Ramp up	$980°C$	Ar(280 sccm) and H_2 (36 sccm)	20
2	Annealing	$980°C$	Ar(280 sccm) and H_2 (36 sccm)	60 minutes
3	Growth	$980°C$	Ar(280 sccm) and CH_4 (variable)	variable
4	Ramp down (Natural)	$450°C$	Ar(280 sccm) and H_2 (36 sccm)	90 minutes
5	Ramp down (furnace opened)	Below $200°C$	Ar(280 sccm) and H_2 (36 sccm)	30 minutes

[67]. During growth step, H_2 was closed and CH_4 supply was turned on. After graphene growth, sample was allowed to cool down naturally under Ar and H_2 protection until the temperature reached $450°C$ and the furnace was opened completely at that time. H_2 is known to etch graphene at higher temperatures [73] so furnace was opened at $450°C$ to reduce the cooling time of the sample so that overall time of graphene interaction with H_2 after the growth step may be reduced. Sample was unloaded when the temperature reached below $200°C$.

<center>Effect of flow rate of precursor and growth time on

graphene growth</center>

In order to study the effect of precursor flow rate and growth time on graphene growth, two flow rates of CH_4 were chosen i.e. *10 sccm* and *20 sccm* while three growth times were selected for each flow rate i.e. *5, 10* and *20 minutes* respectively. Growth temperature was fixed at *980°C* for all conditions. Flow rates of H_2 and Ar were *36 sccm* and *280 sccm* and they were kept constant. Table 8 summarizes the conditions for this set of experiments. Raman spectra were acquired on graphene on copper without the transfer

Table 8.   Conditions for graphene growth for initial set of experiments. I_{2D}/I_G peaks ratios extracted from point scans in Fig. 9 are reported.

Sample Number	Growth Temperature (°C)	CH_4Flow Rate (sccm)	Growth time (minutes)	I_{2D}/I_G
1	980	10	5	1.08
2	980	10	10	0.94
3	980	10	20	0.87
4	980	20	5	1.04
5	980	20	10	0.453
6	980	20	20	0.34

step. The Raman spectra in this study were acquired with Nicolet Almega XR Dispersive Raman spectrometer manufactured by Thermo Scientific Fisher, located in Central Microscopy facility at University of Iowa. *532 nm* laser was used for all the spectra. All point scans were obtained with *100x* microscope objective that corresponds to *0.6 μm* spot size. Each point scan was an average of *5 spectra* taken at random locations across the sample and individual spectrum was an average of *4 exposures* each of duration *15 seconds*. Laser power for each point scan was *2.5 mW* and spectral resolution was *4.0 cm^{-1}-4.9 cm^{-1}*. Fig. 8 shows point scan corresponding to sample number 1 in Table 8. Raman spectrum of as grown graphene on copper shows fluorescence [74] but peaks in the graphene Raman spectrum are clearly identified. This background can be easily subtracted within the control software hence forth all the Raman spectra will be shown with copper background subtracted. Fig. 9 shows Raman point scans corresponding to conditions in Table 8. The most important peaks in the Raman spectrum are the *D, G* and *2D* peaks which occur at approximately *1350 cm^{-1}, 1580 cm^{-1}* and *2700 cm^{-1}* for ideal monolayer graphene as mentioned previously. Since Raman spectra were acquired on
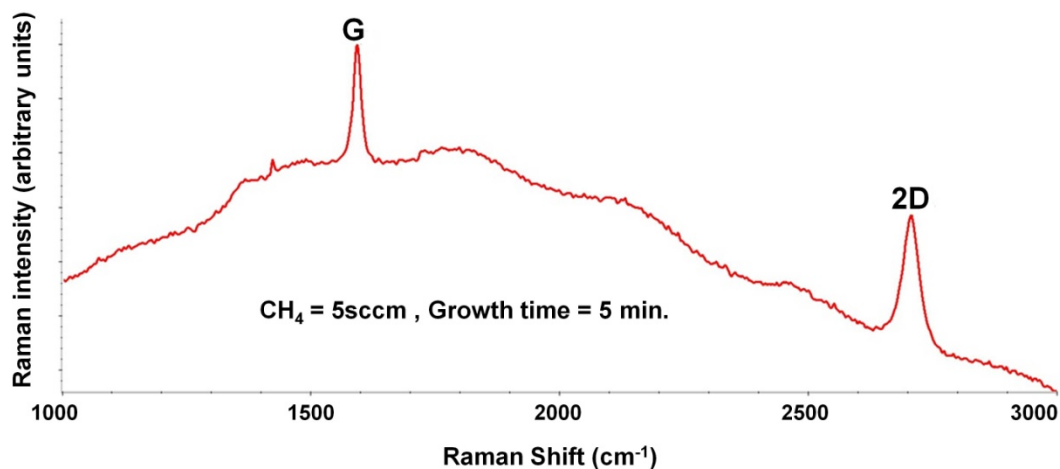
Figure 8. Raman spectrum of graphene on copper. Spectrum shows fluorescence but important peaks in the spectrum can be identified.

copper substrate, the peak locations are shifted [75]. The peaks ratio I_{2D}/I_G is good measure since this ratio is strongly affected by layer number even for graphene on different substrates [76,77]. Fig. 9 shows that for both the flow rates, the peaks ratio I_{2D}/I_G ratio decreases as the growth times increases which indicates that the number of graphene layers increase with the growth time. This observation is different than
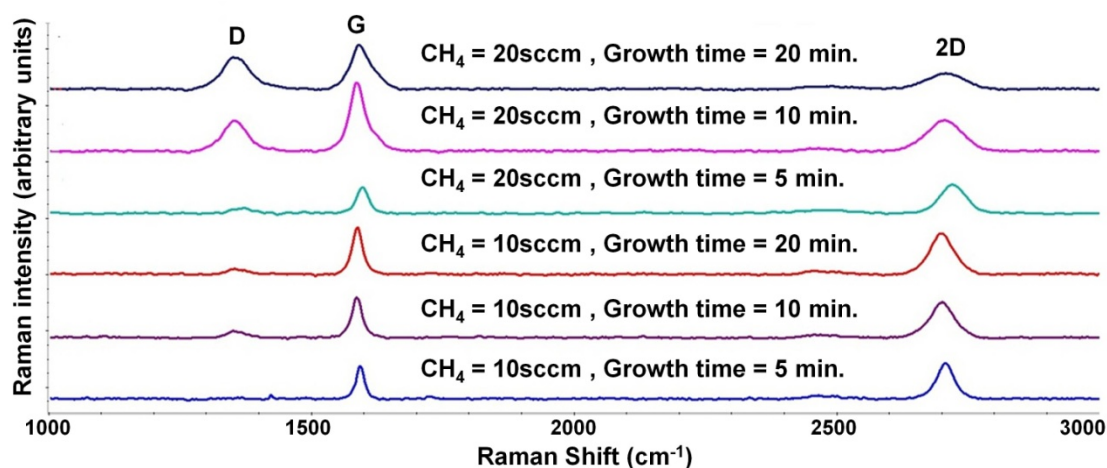
Figure 9. Raman spectra for various growth times with two different CH_4 flow rates. Bilayer graphene is obtained ($I_{2D}/I_G \approx 1$) with *5 minutes* of growth time for both the flow rates. Rest of the spectra show few layer graphene synthesis ($I_{2D}/I_G < 1$). Defect peak is low when both the flow rate and growth time are lower.

graphene grown on copper under low pressure chemical vapor depostion (LPCVD) where graphene growth is self limiting process over wide parameter range [42,43]. From Table 8, the peaks ratio $I_{2D}/I_G \approx 1$ when the growth time was *5 minutes* for both the flow rates which indicates that bilayer graphene [47,78] was obtained under these conditions while peaks ratio $I_{2D}/I_G < 1$ indicates that few layer graphene [42,47,79] was obtained on the rest of samples. Another observation from Table 8 is that for higher flow rate of *20 sccm*, the peaks ratio I_{2D}/I_G falls very quickly with growth time as compared to lower flow rate

of *10 sccm* under same conditions which means that lower flow rate is an important factor in controlling number of layers under APCVD. Fig. 9 also shows that the Defect (*D*) peak increase in intensity as the growth time increase and number of layer increase. From these experiments we conclude that lower flow rate of precursor as well lower growth time are important parameters in decreasing number of layers during the growth step and improving the quality in terms of defects.

<div align="center">Effect of temperature on graphene growth</div>

To study the effect of temperature on graphene growth, the temperature was varied between *900 - 980°C* range, while lower flow rate (*5 sccm*) and lower growth time (*2 min*) were chosen based on results of previous experiments. Table 9 summarizes the growth conditions. The Raman spectra corresponding to these growth conditions are shown in Fig. 10 which indicates that number of layer show strong temperature dependence as seen by sharp increase of the peaks ratio I_{2D}/I_G with increase in temperature. Also the defect peak shows sharp temperature dependence with its intensity decreasing as the temperature increase. From Table 9, the peak ratio I_{2D}/I_G of *1.12* indicates that graphene was still bilayer [78] even for the highest growth temperature of *980°C*. The conclusion of this set of experiments was that higher growth temperatures important in reducing number of graphene layers as well as defects. This temperature

Table 9.   Graphene growth parameters with varying temperature and I_{2D}/I_G peaks ratios extracted from point scans in Fig. 10 are reported.

Sample Number	Growth Temperature ($^\circ$C)	CH_4 Flow Rate (sccm)	Growth time (minutes)	I_{2D}/I_G
7	900	5	2	0.59
8	950	5	2	0.78
9	980	5	2	1.12
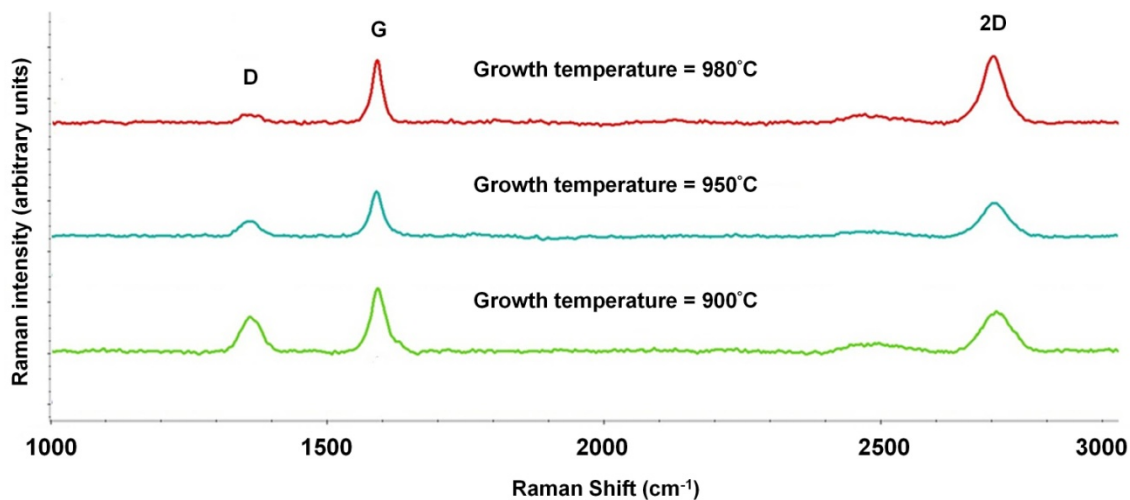
Figure 10. Raman spectra for various growth conditions. Bilayer graphene is obtained at 980°C ($I_{2D}/I_G = 1.12$) while few layer graphene ($I_{2D}/I_G < 1$) is synthesized for all other growth temperatures. Defects in the synthesized graphene also reduce at higher growth temperature.

dependence is in general in agreement with growth of thin films which shows crystalline behavior when grown at elevated temperature while amorphous growth at lower growth temperatures [80]. The reduction in the number of graphene layers as well as defects with temperature can be understood from the fact that graphene growth on copper is surface catalysis process [39,44] due to small solubility of carbon in copper even at elevated temperatures [13]. Graphene growth on copper proceeds by nucleation step [54,55] similar to thin film growth. At lower growth temperatures the mobility of ad-atoms that leads to thin film growth is low on the substrate [81,82] which means that before they can get attached to already growing sites on the substrate, additional ad-atoms get deposited onto them because of the continuous decomposition of precursor (CH_4 in our case). As the growth temperature increase the mobility of these ad-atoms increase and they get attached to more favorable sites before getting covered by additional ad-atoms with the overall result that growth is more crystalline at elevated temperatures.

To see the spatial variation of number of layers across the substrate, Raman area maps were also acquired. Growth temperature of *1000°C,* flow rate of *5 sccm* and growth time of *30 seconds* were selected based on previous observations that higher growth temperature and lower flow rate and growth time leads to higher peaks ratio I_{2D}/I_G . Table 10 shows these growth conditions while Raman area maps are shown in Fig.11. Spatial area maps were acquired over *100 μm × 100 μm* area with *20x* objective that corresponds

Table 10. Growth conditions when Raman area maps were acquired to study the spatial uniformity of graphene layers. Range of I_{2D}/I_G peaks ratio in the area map is also reported.

Sample Number	CH$_4$ Flow Rate (sccm)	Growth Temperature (°C)	Growth Time (seconds)	I$_{2D}$/I$_G$
10	5	1000	30	0.4 – 4.0
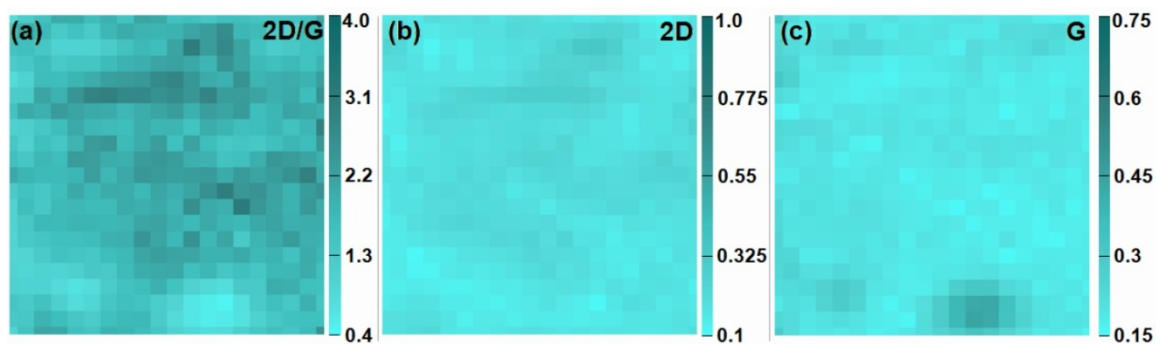
Figure 11. Raman area maps. (a) Spatial mapping of *2D/G* peaks ratio which show variation in number of graphene layers (I_{2D}/I_G = *0.4 – 4*). (b,c) Spatial mapping of the intensity of *2D* and *G* peaks respectively. Area in each Raman map correspond to *100 μm × 100 μm* with *5 μm × 5 μm* pixel size.

to *1.2 μm* spot size. Laser power was *3.75 mW* and individual spectrum in the area map was an average of *4 exposures* each of duration *15 seconds*. Collection parameters were same for all area maps. Spatial mapping of the specific peak was obtained after selecting

reference spectrum in the control software. From Fig.11, the scale bar of I_{2D}/I_G peaks ratio varies from *0.4 - 4.0* which indicate that monolayer along with bilayer and few layer graphene were present on this sample. Based on pixel account approximately *20%* of the given scanned area contained monolayer graphene corresponding to $I_{2D}/I_G > 2$ [42,43,55] while the rest of the given area was covered with bilayer and few layer graphene.

Effect of fast sample cooling on graphene growth

To study the effect of fast sample cooling on graphene growth, the hot quartz tube was moved out of the furnace immediately after closing the precursor gas (CH_4). Table 11 summarizes the growth conditions. After the growth step, graphene was also transferred to *300 nm* SiO_2/Si substrate, to study changes in the Raman spectrum after the transfer step. Graphene was transferred following the procedure in Chapter 2. Fig. 12 shows Raman area maps corresponding on this sample. Each Raman map represents spatial area of *150 μm ×150 μm* with *10 μm ×10 μm* pixel size. The I_{2D}/I_G peaks ratio in Fig. 12(a) varies from *0.4 – 4.0* which shows that there was still variation in terms of number of layers in the given area. Based on pixel count, approximately *35%* of the scanned area contained monolayer graphene with $I_{2D}/I_G > 2$. The *D* peak intensity was small in the given area which indicates good quality transfer. Another observation from this sample is shown by Raman point scans in Figs. 13(a,b,c) after the transfer step. From the I_{2D}/I_G peaks ratio, (a) represents few layer graphene with $I_{2D}/I_G < 1$, (b) represents monolayer graphene with $I_{2D}/I_G > 2$ and (c) represents bilayer graphene with $I_{2D}/I_G \approx 1.2$. This variation in Raman spectra was due to rolling marks on the underlying copper foils as reported by others. [46,47]. These features on copper foil are developed due to the cold rolling process during manufacture [83,84]. Because of these marks, copper surface is not smooth and contains step edges which represent surface irregularities. Since graphene growth on copper is surface catalysis process [44], graphene preferentially nucleates on these step edges because such irregularities on the atomic scale contain dangling bonds

which present lower energy barrier for attachment to the ad-atoms that govern graphene growth [39]. The result is that for the same growth time stepped regions contain few layer graphene compared to smooth copper surface. Though annealing of copper at higher temperatures mitigate the effect of such surface irregularities [48] but that was not enough to remove their effect as seen by bilayer and few layer graphene growth along these rolling marks, confirmed by Raman spectra of the transferred graphene in Fig. 13.

<div align="center">Graphene growth on foil with evaporated copper film</div>

To overcome previous problem, copper film was evaporated on the copper foil before graphene growth. Table 12 summarizes the modified recipe for this set of experiments. After performing the initial solvent cleaning step, the copper foils were annealed in H_2 and Ar gas mixture to remove native copper oxide similar to previous recipe. After annealing step, foils were allowed to cool down naturally under H_2 and Ar protection to avoid oxidation of copper. Then *900 nm* copper film was evaporated by electron beam evaporation following the procedure mentioned in Chapter 2. After evaporation, the sample was loaded into the quartz tube of CVD furnace and the temperature was ramped up to the growth temperature of *1000°C*. Conditions for graphene growth are mentioned in Table 13. Flow rate of CH_4 was *5 sccm* and the growth time was *2 minutes*. After growth sample was fast cooled by quenching the hot tube out of furnace. Sample was unloaded approximately half an hour after the growth step and graphene was transferred onto *300 nm* SiO2/Si. Raman area maps were collected on *150 μm × 150 μm* area on this sample and they are shown in Fig 14. Size of each pixel is *10 μm × 10μm*. For comparison area maps on copper foil without evaporated film are also shown from Fig. 12 that was prepared under same growth conditions. The bottom row in Fig. 14 shows Raman area maps for graphene grown on copper foil without evaporated film while top row shows area map for graphene grown on copper foil with *900 nm* evaporated copper film. From Fig. 14(a), I_{2D}/I_G peaks ratio corresponding to graphene

Table 11. Growth conditions for fast cooling. Range of I_{2D}/I_G peaks ratio in the area map is reported as well.

Sample Number	Growth Temperature (°C)	CH$_4$ Flow Rate (sccm)	Growth Time (minutes)	I$_{2D}$/I$_G$
11	1000	5	2	0.4 – 4.0
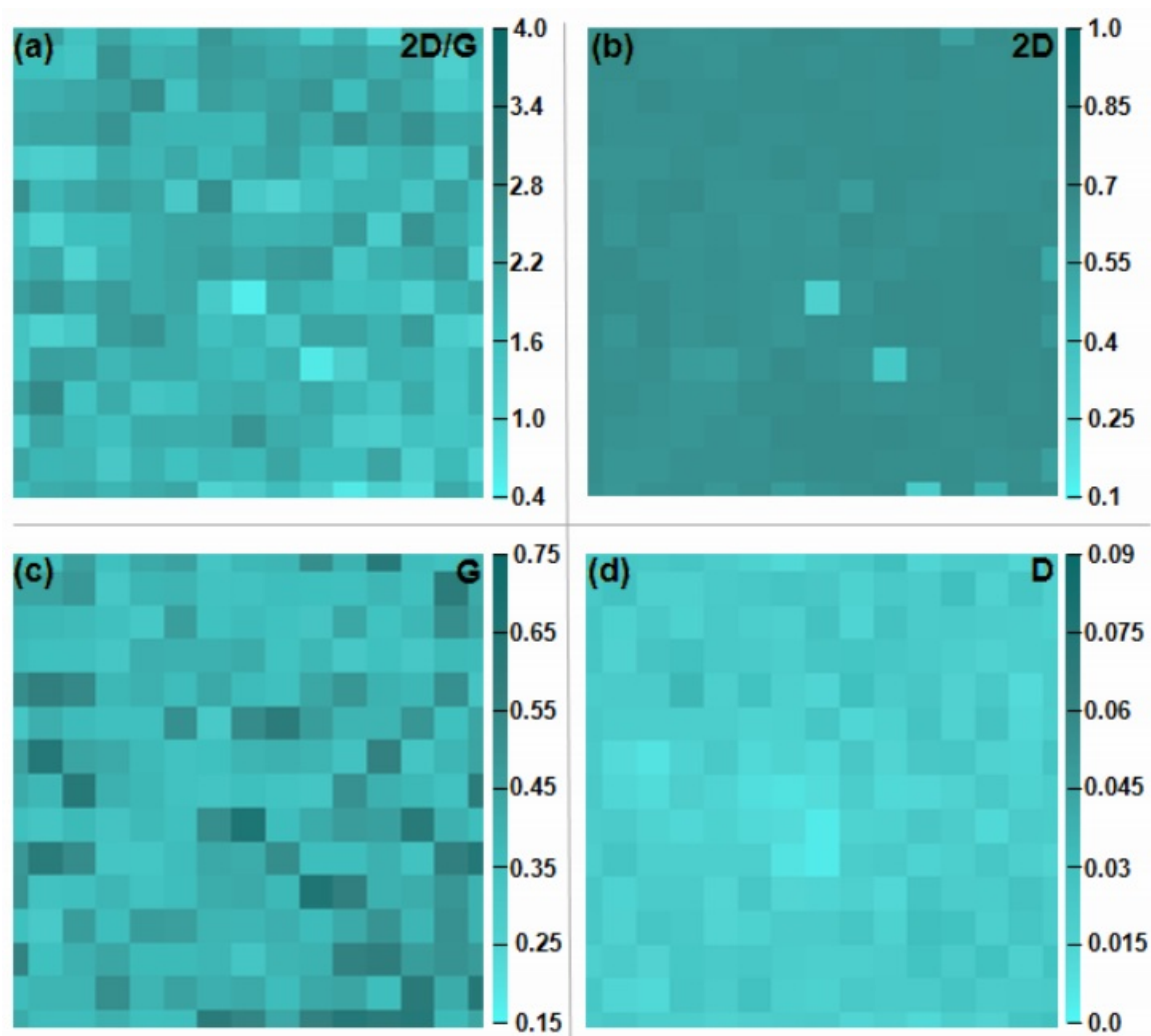
Figure 12. Raman area maps. (a) Spatial mapping of *2D/G* peaks ratio which show variation in number of graphene layers ($I_{2D}/I_G = 0.4 – 4$). (b,c,d) Spatial mapping of the intensity of *2D, G* and *D* peaks respectively. Area in each Raman map correspond to *150 μm×150 μm*. with *10 μm×10 μm* pixel size.
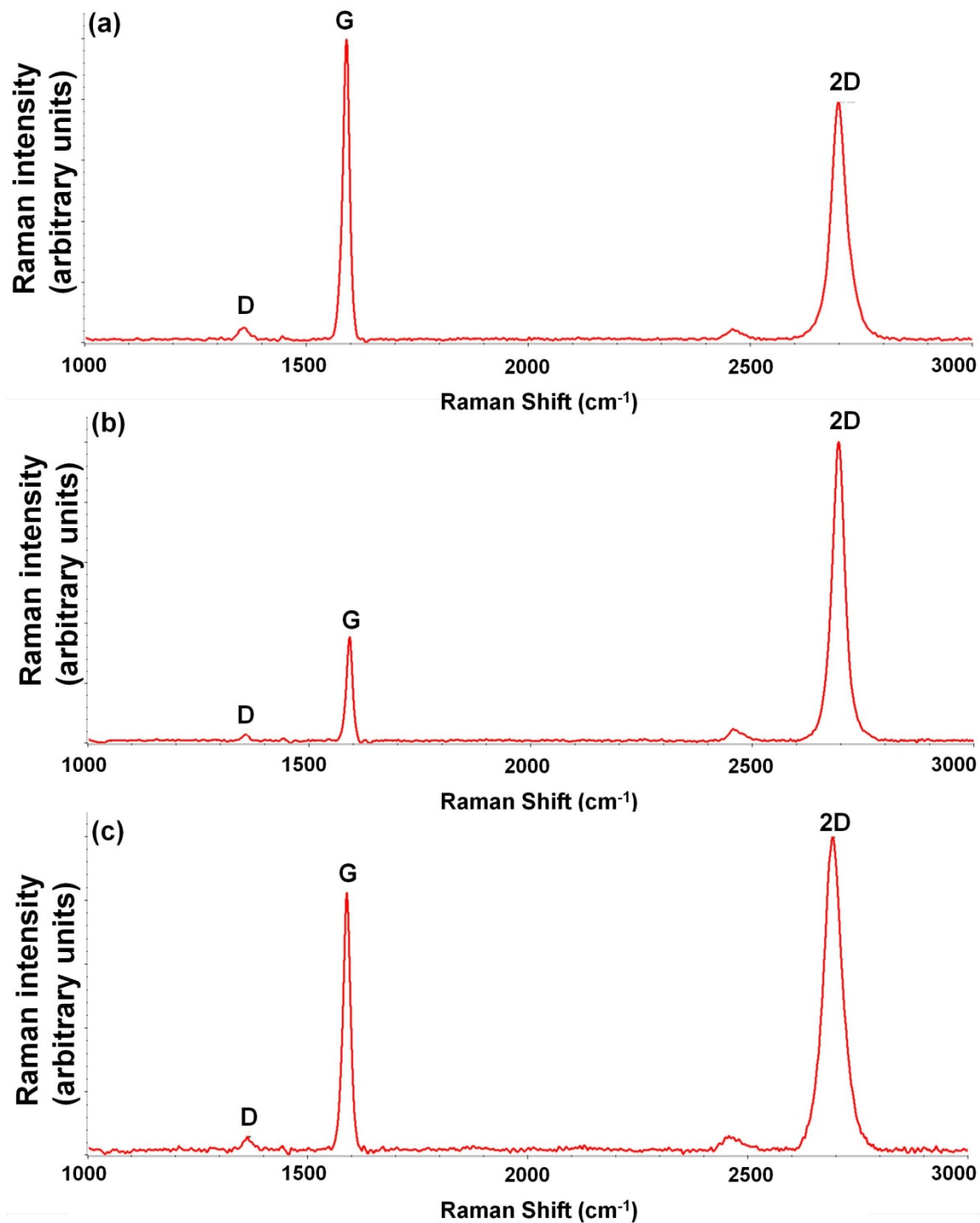
Figure 13. Raman point scans for transferred graphene synthesized on foil. (a) few layer graphene $(I_{2D}/I_G < 1)$. (b) monolayer graphene $(I_{2D}/I_G > 2)$. (c) bilayer graphene $(I_{2D}/I_G \approx 1.2)$.

Table 12. Modified recipe for graphene growth.

Step Number	Processing step	Temperature	Processing gases	Duration (minutes)
1	Ramp up	1000$°$C	Ar (280 sccm) and H$_2$(36 sccm)	20
2	Annealing	1000$°$C	Ar (280 sccm) and H$_2$(36 sccm)	120
3	Ramp down (Natural)	Room temperature	Ar (280 sccm) and H$_2$(36 sccm))	360
4‡	Ramp up	1000$°$C	Ar (280 sccm) and H$_2$(36 sccm)	20
5	Growth	980$°$C	Ar (280 sccm) and CH$_4$(variable)	variable
6	Ramp down (Fast Cooling)	Below 800$°$C	Ar (280 sccm)	<3

Table 13. Graphene growth conditions for foil with *900 nm* evaporated copper film.

Sample Number	Growth Temperature ($°$C)	CH$_4$ Flow Rate (sccm)	Growth time (minutes)
12	1000	5	2

grown on *900 nm* evaporated copper film, is greater than *2* for all the pixels which indicates monolayer graphene in the given scanned area. The I_{2D}/I_G peaks ratio in Fig. 14(e) for graphene grown on copper foil without evaporated film shows variation from from *0.4 – 4.0*, which shows the presence of bilayer and few layer along with monolayer graphene as discussed previously. The intensity of *D* peak is low for the both samples which indicate good quality after the transfer step. Raman points scans were also

---

‡ Before this step copper thin film was evaporated
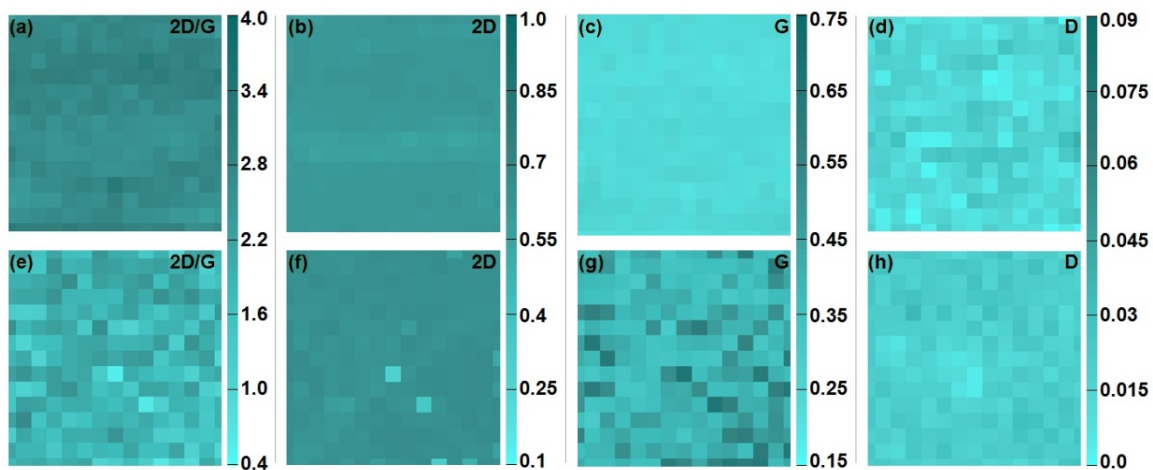
Figure 14. Raman area maps for various growth conditions. Top and bottom rows are for graphene grown *900 nm* evaporated copper film/foil and copper foil respectively (a,e) Spatial mapping of *2D/G* peaks ratio. (b,f) Spatial mapping of the intensity of *2D* peak. (c,g) Spatial mapping of the intensity of *G* peak. (d,h) Spatial mapping of the intensity of *D* peak. (a) shows complete monolayer coverage for graphene grown on foil with *900 nm* evaporated film ($I_{2D}/I_G > 2$). Area in each Raman map correspond to *150 μm×150 μm* with *10 μm×10 μm* pixel size.

acquired on this sample and they are shown in Figs. 15(a,b,c). The I_{2D}/I_G peaks ratio is greater than *2* in all three locations confirming monolayer graphene. This shows that *900 nm* evaporated copper film was enough to cover the step edges on the underlying copper foil and presented smooth surface for graphene growth.

<div align="center">

Effect of growth time on graphene growth on foil with

evaporated copper film

</div>

To see the minimum growth time, graphene was grown under *1.5 minutes* of growth time. Growth temperature and CH$_4$ flow rate were fixed at *1000°C* and *5 sccm* respectively. Table 14 summarizes these growth conditions. The corresponding Raman point scans are shown in Fig.16. Raman spectrum from previous study i.e. Sample 12 in Table 13 is also included for comparison, which was prepared under same conditions with the only
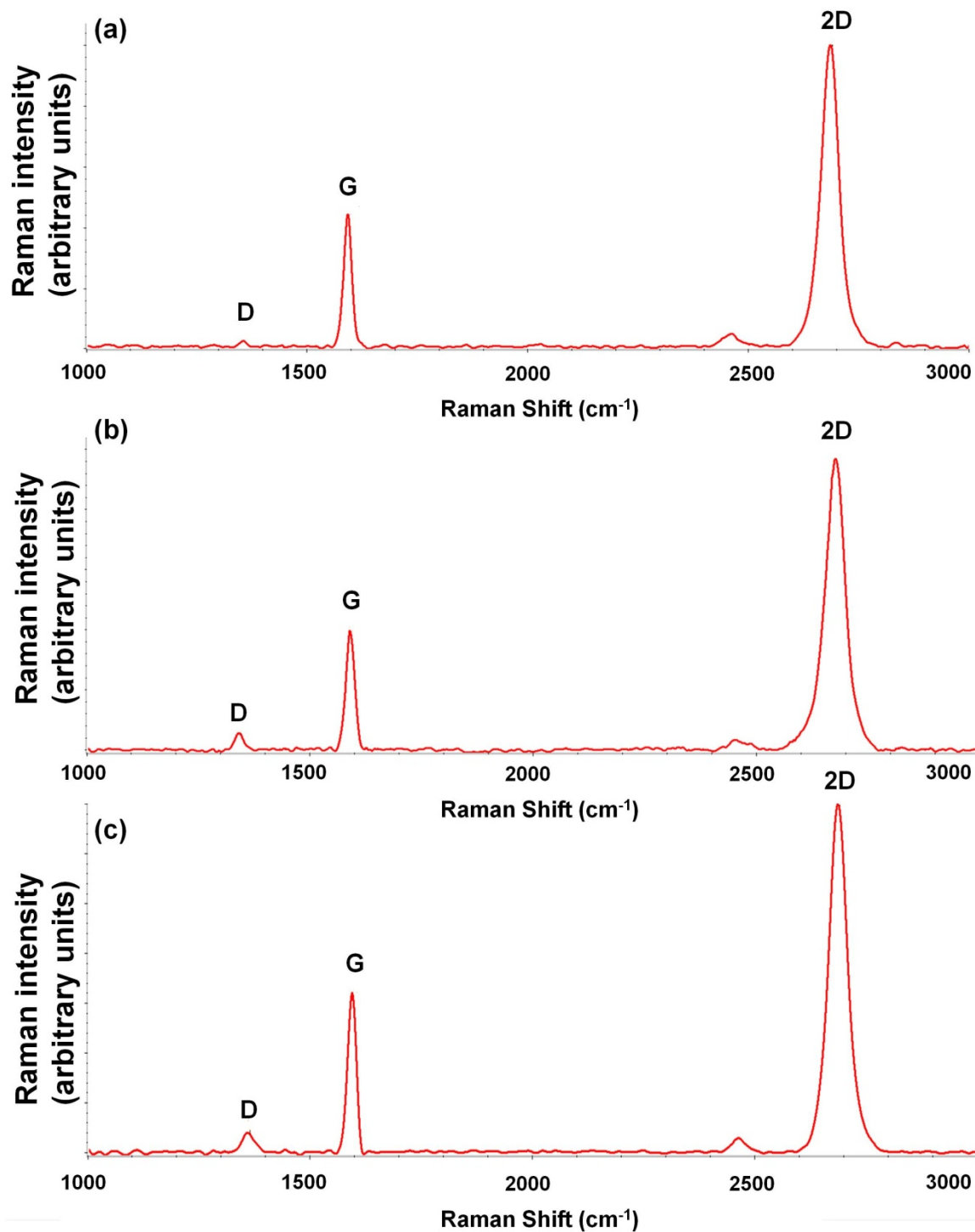
Figure 15. Raman point scans for transferred graphene synthesized on *900 nm* copper film on foil. (a,b,c) monolayer graphene ($I_{2D}/I_G > 2$).

difference that growth time was *2 minutes*. The data extracted from these point scans is shown in Table 15, which shows that monolayer graphene was also obtained even for *1.5 minutes* of growth time as indicated by the I_{2D}/I_G peaks ratio of *2.5*. *2D* peak positions in Table 15 are consistent for CVD grown monolayer graphene on copper and transferred to SiO$_2$/Si [79,85,86]. The blue shift in the *G* peak position relative to ideal position of *1580 cm^{-1}* is due to doping induced by the SiO$_2$/Si [72]. The blue shift of ~ *10 cm^{-1}* in G peak as seen from Table 15 for both the samples suggests doping of the order of *10^{12} cm^{-3}* [87]. Defect peak intensity is low for the both the samples which indicates good quality.

Table 14. Graphene growth conditions for foil with *900 nm* evaporated film when growth time was varied.

Sample Number	Growth Temperature ($^{\circ}$C)	CH$_4$ Flow Rate (sccm)	Growth time (minutes)
13	1000	5	1.5
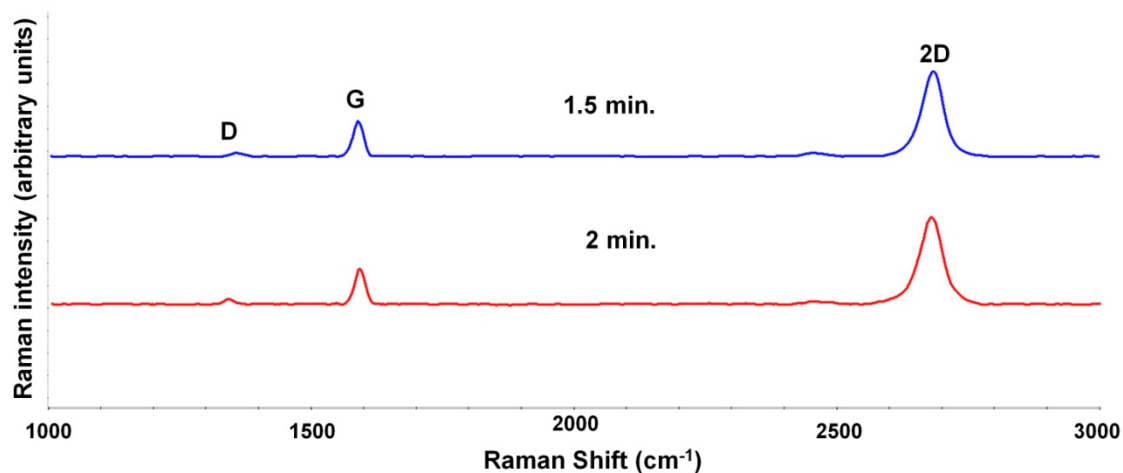
Figure 16. Raman point scans for graphene grown on *900 nm* copper film/foil with various growth times. Monolayer graphene is obtained for *1.5* and *2 minutes* of growth *(I_{2D}/I_G > 2)*.

Table 15. Position and intensities of important peaks extracted from Raman points scan in Fig. 16

Sample Number	Growth Time (minutes)	G peak Position (cm^{-1})	2D peak Position (cm^{-1})	D peak Position (cm^{-1})	I_{2D}/I_G
13	1.5	1588	2682	1356	2.5
12	2	1592	2684	1355	2.3

Effect of variation in thickness of evaporated copper film

on graphene growth

To see the minimum thickness of evaporated copper film for monolayer graphene growth, two values of evaporated film thickness were chosen i.e. *300 nm* and *100 nm*. Growth parameters are summarized in Table 16. After growth, samples were fast cooled and graphene was transferred to *300 nm* SiO$_2$/Si for Raman study. Raman area maps were collected over *150 μm ×150 μm* area on each sample and they are shown in Fig. 17. The top and bottom rows in Fig. 17 are for graphene grown on *300 nm* and *100 nm* evaporated copper film respectively. *I$_{2D}$/I$_G$* peaks ratio is greater than *2* for all pixels in Fig 17(a) which indicates monolayer graphene growth on *300nm* evaporated copper film but for graphene grown on *100 nm* copper film, approximately *10%* of the pixels show *I$_{2D}$/I$_G$*

Table 16. Graphene growth conditions for foil with various thickness of evaporated copper film.

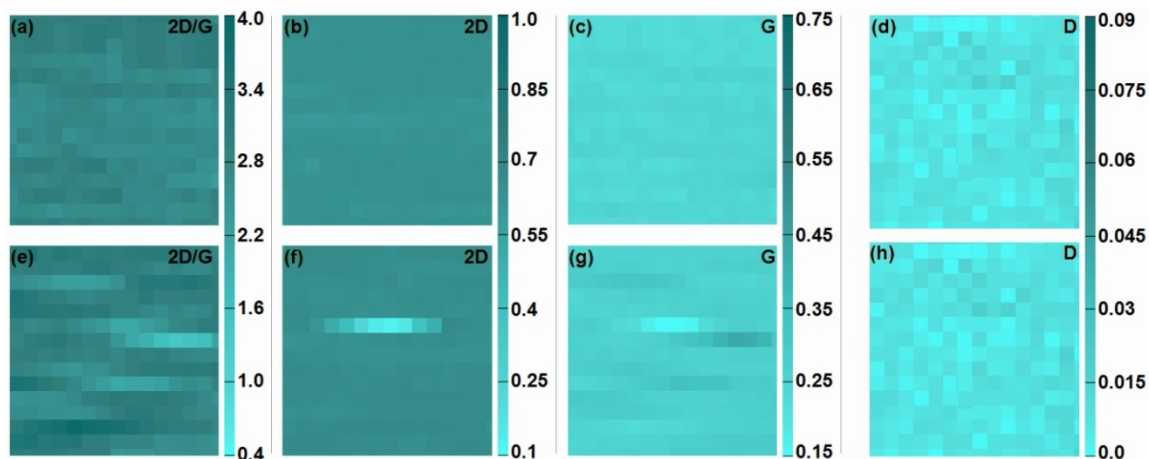| Sample Number	Evaporated Copper film thickness (nm)	Growth Temperature (°C)	CH$_4$ Flow Rate (sccm)	Growth time (minutes)
14	100	1000	5	2
15	300	1000	5	2

Figure 17. Raman area maps for various growth conditions. Top and bottom rows are for graphene grown on foil with *300* and *100 nm* copper films respectively. (a,e) Spatial mapping of *2D/G* peaks ratio, (b,f) Spatial mapping of the intensity of *2D* peak. (c,g) Spatial mapping of the intensity of *G* peak. (d,h) Spatial mapping of the intensity of D peak. (a) shows complete monolayer coverage for graphene grown on foil with *300 nm* evaporated film ($I_{2D}/I_G > 2$). (e) shows mix of monolayer and multilayer for graphene grown on foil with *100 nm* evaporated film($I_{2D}/I_G = 0.4 – 4.0$). Area in each Raman map correspond to *150 μm ×150 μm* with *10 μm ×10 μm* pixel size.

peaks ratio less than *2*. The minimum scale bar is *0.4* which means monolayer and multi layers were present when graphene was grown on *100 nm* evaporated film. This indicates that the copper film thickness was too small to counter the effect of rolling marks on the underlying copper surface and step edges on the underlying copper foil even after annealing were greater than *100 nm*. The *D* peak intensity for all the samples was low which showed good quality transfer. Based on conclusion of this experiment, that monolayer graphene was obtained even with *300 nm* copper film, the optimal sample in this study was prepared with this minimum thickness under the growth conditions mentioned in Table 17. Growth time of *1.5 minutes* was selected based on previous results and after the transfer step, Raman area maps were obtained on relatively larger area compared to previous area maps i.e *300 μm ×300 μm* and they are shown in Fig. 18. Size of each pixel in individual Raman map is *20 μm ×20 μm*. The scale bar of I_{2D}/I_G

peaks ratio in Fig. 18(a) is greater than *2* for all pixels which indicate single layer graphene across the entire *300 μm ×300 μm* area while the defect intensity was also low. Table 18 compares I_{2D}/I_G peaks ratios and *2D* peak positions for graphene synthesized on copper in this study with earlier reports for the same precursor i.e CH_4. From Table 18, the I_{2D}/I_G peaks ratios and *2D* peak positions for monolayer graphene obtained in this study are in agreement with earlier work.

Table 17. Graphene growth conditions for graphene growth on foil with *300 nm* evaporated copper film.

Sample Number	Evaporated Copper film thickness (nm)	Growth Temperature ($^\circ$C)	CH_4 Flow Rate (sccm)	Growth time (minutes)
16	300	1000	5	1.5
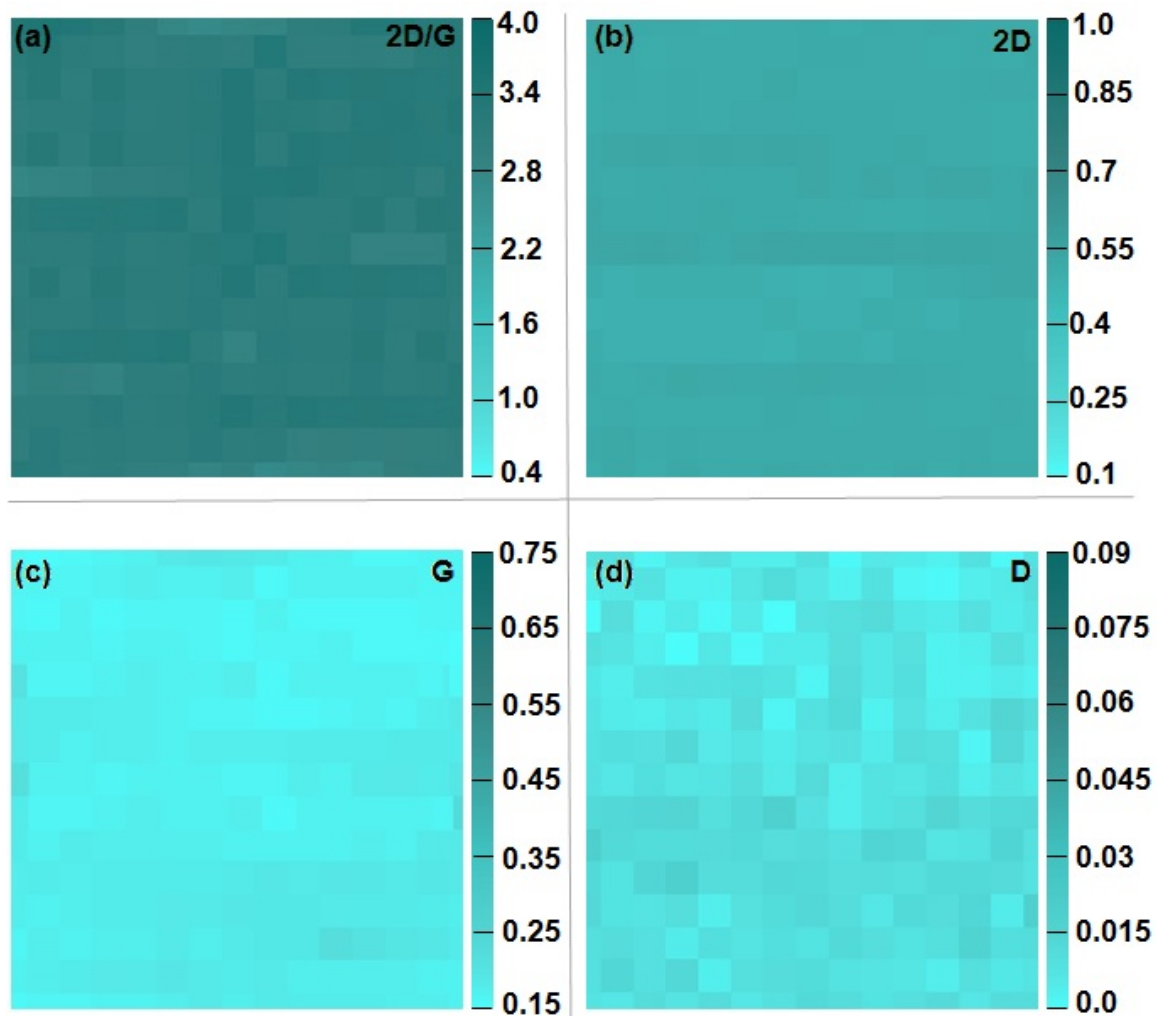
Figure 18. Raman area maps for graphene grown on foil with *300 nm* copper film. (a) Spatial mapping of *2D/G* peaks ratio which shows complete monolayer coverage ($I_{2D}/I_G > 2$). (b,c,d) Spatial mapping of the intensities of *2D, G* and *D* peaks respectively. Area in each Raman map correspond to *300 μm×300 μm* with *20 μm×20 μm* pixel size.

.

Table 18. Comparison of I_{2D}/I_G peaks ratio and *2D* peak position of monolayer graphene obtained in this study with earlier work.

Graphene grown on copper foils	I_{2D}/I_G	2D peak position (cm^{-1})	Growth Temperature$(°C)$	Growth technique
This study	2.2-3.4	2680-2685	1000	APCVD
Ref. 42	2	2680	1000	LPCVD
Ref. 46	>2	2670	1000	LPCVD
Ref. 48	2-3.2	2640	1000	LPCVD
Ref. 53	2.5-4	2698	1120	LPCVD
Ref.55	>2	2690	1000	APCVD
Ref. 75	2.9	2695	1000	LPCVD
Ref. 88	2.84	2690	1070	APCVD
Ref. 89	2.5	2687	1050	APCVD
Ref. 90	3	2689	1045	APCVD
Ref. 91	>1	2643-2648	1000	APCVD
Ref. 92	3-5	2686-2700	1000	APCVD

CHAPTER IV

SUMMARY AND FUTURE WORK

Summary

The goal of this project was to optimize monolayer graphene synthesis and transfer process using our home made hot wall atmospheric pressure chemical vapor deposition (APCVD) system. CVD was selected as synthesis technique for graphene growth as it is a low cost method for large scale graphene synthesis and also the yield is very good compared to the other growth methods. Copper foils were chosen as substrate for growth because of the lower solubility of carbon in copper [13] which is important in controlling number of graphene layers. CH_4 was used was precursor gas while H_2 annealing was used to remove native oxide as well as to grow copper grains. Ar acted as carrier gas during synthesis to dilute the precursor gas. Raman spectroscopy was used as characterization technique as graphene shows characteristic Raman spectrum which can be used to distinguish number of layers on a given sample. After initial experiments on copper foils it was found that graphene growth on copper under APCVD is non self limiting process and monolayer graphene along with bilayer and few layer formed non uniformly even with the lowest flow rate of precursor, lower growth time and higher growth temperatures. Fast cooling was also applied to limit the growth time after the precursor supply is stopped but still obtained graphene was non uniform across the copper substrate. To get further insight, graphene was transferred onto insulating substrate i.e. *300 nm* SiO_2/Si. Graphene transfer process was optimized using *AZ9260* Photoresist and scotch tape as handle layer. Graphene obtained after transfer showed good quality confirmed by Raman spectroscopy which showed minimum defects induced after the transfer process. After transfer process, it was confirmed by Raman microscopy that bilayer and few layer graphene nucleated along the corrugations on the underlying

copper foil. These marks are developed on copper foils during their manufacture [83,84]. Though high temperature thermal annealing reduce the effect of such surface irregularities [48] but that was not enough to completely remove those rolling marks. To overcome this problem, copper film was evaporated on copper foil by electron beam evaporation. Initially *900 nm* film was evaporated and after graphene growth and transfer, Raman area maps confirmed monolayer graphene coverage across *150 μm × 150 μm* area. It was found that minimum thickness of evaporated copper film for uniform monolayer graphene growth was *300 nm*. Graphene wss also grown on *100 nm* evaporated copper film but it showed both bilayer and monolayer graphene which indicates that step edges on the copper foil even after annealing were higher than *100 nm* and thickness of evaporated film was not sufficient to counter their effect.

Future work

Since the ultimate goal of graphene synthesis is to employ graphene into nanoelectronic devices the next step will be to optimize graphene transistor fabrication process and to extract and optimize parameters which are important from electronic devices point of view e.g. mobility , current density. A potential application of graphene is in non volatile memory devices so memory devices will be fabricated with graphene as storage medium to compare their performance with the state of the art non volatile memory devices.

Pristine monolayer graphene itself has zero bandgap which means that transistor made out of graphene cannot be turned off which is problem for devices geared towards logic applications. Bandgap can be induced in graphene by reducing the dimensions of graphene sheet thus turning into graphene nano ribbons. Experiments will also be done to fabricate graphene nano ribbons made out of graphene sheet so that they can be employed as channel material in the nano scale field effect transistors.

REFERENCES

1. Moore, G. *Solid-State Circuits Conference,* **2003***, 1,* 20-3.

2. Schwierz, F. *Nat. Nanotech.* **2010**, *5*, 487-496.

3. Geim, A. K.; Novoselov, K. S. *Nat. Mater.* **2007**, *6*, 183-191.

4. Novoselov, K. S.; Geim, A K.; Morozov, S. V.; Jiang, D.; Zhang, Y.; Dubonos, S. V.; Grigorieva, I. V.; Firsov, *Science* **2004**, *306*, 666-669.

5. Bolotin, K. I.; Sikes, K. J.; Jiang, Z.; Klima, M.; Fudenberg, G.; Hone, J.; Kim, P.; Stormer, H. L. *Solid State Commun.* **2008**, *146*, 351-355.

6. Moser, J.; Barreiro, A.; Bachtold, A. *Appl. Phys. Lett.* **2007**, *91*, 163513

7. Nair, R. R.; Blake, P.; Grigorenko, A. N.; Novoselov, K. S.; Booth, T. J.; Stauber, T.; Peres, N. M. R.; Geim, A. K. **2008**, *Science 320*, 2008.

8. Balandin, A. A.; Ghosh, S.; Bao, W.; Calizo, I.; Teweldebrhan, D.; Miao, F.; Lau, C. N. **2008**, *Nano Lett. 8(3),*902-907.

9. Novoselov, K. S.; Jiang, D.; Schedin, F.; Booth, T. J.; Khotkevich, V. V.; Morozov, S. V.; Geim, A K. *Proc. Natl. Acad. Sci.* **2005**, *102*, 10451-3.

10. Raza, M. *Graphene Nanoelectronics Metrology, Synthesis, Properties and Applications*, Springer-Verlag ; Berlin Heidelberg, **2012.**

11. Geim, A. K. *Science* **2009**, *324*, 1530-4

12. Obraztsov, A.N. *Nat.Nanotech.* 2009, *4*, 212-213

13. López, G. A.; Mittemeijer, E. J. *Scripta Mater.* **2004**, *51*, 1-5.

14. Lemme, M. C. *Solid State Phenom.* **2009**, *156-158*, 499-509.

15. Castro Neto, A. H.; Peres, N. M. R.; Novoselov, K. S.; Geim, A. K. *Rev. Mod. Phys.* **2009**, *81*, 109-162.

16. Raza, H.; *Nanoelectronics Fundamentals*, unpublished.

17. Zhang, Y.; Small, J. P.; Pontius, W. V.; Kim, P. *Appl. Phys. Lett.* **2005**, *86*, 073104.

18. Blake, P.; Hill, E. W.; Castro Neto, A. H.; Novoselov, K. S.; Jiang, D.; Yang, R.; Booth, T. J.; Geim, A. K. *Appl. Phys. Lett.* **2007**, *91*, 063124.

19. Soldano, C.; Mahmood, A.; Dujardin, E. *Carbon* **2010**, *48*, 2127-2150.

20. Neugebauer, P.; Orlita, M.; Faugeras, C.; Barra, A.-L.; Potemski, M. *Phys. Rev. Lett.* **2009**, *103*, 2-5.

21. Dean, C. R.; Young, A. F.; Meric, I.; Lee, C.; Wang, L.; Sorgenfrei, S. *Nat. Nanotech.* **2010**, *5*, 722-726.

22. Chen, J.-H.; Jang, C.; Xiao, S.; Ishigami, M.; Fuhrer, M. S. *Nat. Nanotech.* **2008**, *3*, 206-9.

23. Bolotin, K. I.; Sikes, K. J.; Jiang, Z.; Klima, M.; Fudenberg, G.; Hone, J.; Kim, P.; Stormer, H. L. *Solid State Commun.* **2008**, *146*, 351-355.

24. Ishigami, M.; Chen, J. H.; Cullen, W. G.; Fuhrer, M. S.; Williams, E. D. *Nano lett.* **2007**, *7*, 1643-8.

25. Forbeaux, I.; Themlin, J.; Debever, J. *Surf. Sci.* **1999**, *442*, 9-18.

26. Sutter, P. *Nat. Mater.* **2009**, *8*, 171-172.

27. Hass, J.; Feng, R.; Li, T.; Li, X.; Zong, Z.; de Heer, W. A.; First, P. N.; Conrad, E. H.; Jeffrey, C. A.; Berger, C. *Appl.Phys. Lett.* **2006**, *89*, 143106.

28. Emtsev, K. V.; Bostwick, A.; Horn, K.; Jobst, J.; Kellogg, G. L.; Ley, L.; McChesney, J. L.; Ohta, T.; Reshanov, S. A; Röhrl, J.; Rotenberg, E.; Schmid, A. K.; Waldmann, D.; Weber, H. B.; Seyller, T. *Nat. Mater.* **2009**, *8*, 203-7.

29. Park, S.; Ruoff, R. S. *Nat. Nanotech.* **2009**, *4*, 217-24.

30. Lerf, A.; He, H.; Forster, M. *J. Phys. Chem. B* **1998**, *5647*, 4477-4482.

31. He, H.; Riedl, T.; Lerf, A. *J. Phys. Chem. B* **1996**, *3654*, 19954-19958.

32. Buchsteiner, A.; Lerf, A.; Pieper, *J. Phys. Chem. B* **2006**, *110*, 22328-38.

33. Bose, S.; Kuila, T.; Mishra, A. K.; Kim, N. H.; Lee, J. H. *Nanotechnology* **2011**, *22*, 405603.

34. An, X.; Simmons, T.; Shah, R.; Wolfe, C.; Lewis, K. M.; Washington, M.; Nayak, S. K.; Talapatra, S.; Kar, S. *Nano letters* **2010**, *10*, 4295-301.

35. Jiao, L.; Zhang, L.; Wang, X.; Diankov, G.; Dai, H. *Nature* **2009**, *458*, 877-80.

36. Raza, H. *J. Phys:. Condens. Matter* **2011**, *23*, 382203.

37. Raza, H. *Phys.Rev. B.* **2011 ,** *84*, 165425

38. Raza, H. *Physi. Rev. B.* **2008 ,** *77*, 245434

39. Mattevi, C.; Kim, H.; Chhowalla, M. *J. Mat. Chem.* **2011**, *21*, 3324.

40. Kim, K. S.; Zhao, Y.; Jang, H.; Lee, S. Y.; Kim, J. M.; Kim, K. S.; Ahn, J.-H.; Kim, P.; Choi, J.-Y.; Hong, B. H. *Nature* **2009**, *457*, 706-10.

41. Reina, A.; Jia, X.; Ho, J.; Nezich, D.; Son, H. *Nano let.* **2008**, *9*, 30-5.

42. Li, X.; Cai, W.; An, J.; Kim, S.; Nah, J.; Yang, D.; Piner, R.; Velamakanni, A.; Jung, I.; Tutuc, E.; Banerjee, S. K.; Colombo, L.; Ruoff, R. S. *Science* **2009**, *324*, 1312-4.

43. Li, X.; Magnuson, C. W.; Venugopal, A.; Tromp, R. M.; Hannon, J. B.; Vogel, E. M.; Colombo, L.; Ruoff, R. S. *J. Am. Chem. Soc.* **2011**, *133*, 2816–2819.

44. Li, X.; Cai, W.; Colombo, L.; Ruoff, R. S. *Nano lett*. **2009**, *9*, 4268-4272.

45. Congqin, M.; Churan, Z.; Owen, L.; Ya-Hong, X. Chemical Vapor Deposition of Graphene. In *Physics and Applications of Graphene - Experiments*; Mikhailov, S. Ed.; InTech: Rijeka, **2011**,37-54

46. Luo, Z.; Lu, Y.; Singer, D. W.; Berck, M. E.; Somers, L. A.; Goldsmith, B. R.; Johnson, A. T. C. *Chem. Mater.* **2011**, *23*,1441-1447.

47. Liu, W.; Li, H.; Xu, C.; Khatami, Y.; Banerjee, K. *Carbon* **2011**, *49*, 4122-4130.

48. Kim, H.; Mattevi, C.; Calvo, M. R.; Oberg, J. C.; Artiglia, L.; Agnoli, S.; Hirjibehedin, C. F.; Chhowalla, M.; Saiz, E. *ACS nano* **2012**, *6*, 3614-3623.

49. Gomez De Arco, L.; Zhang, Y.; Schlenker, C. W.; Ryu, K.; Thompson, M. E.; Zhou, C. *ACS nano* **2010**, *4*, 2865-2873.

50. Kim, K.; Lee, Z.; Regan, W.; Kisielowski, C.; Crommie, M. F.; Zettl, A. *ACS nano*. **2011**, 2142-2146.

51. Huang, P. Y.; Ruiz-Vargas, C. S.; van der Zande, A. M.; Whitney, W. S.; Levendorf, M. P.; Kevek, J. W.; Garg, S.; Alden, J. S.; Hustedt, C. J.; Zhu, Y.; Park, J.; McEuen, P. L.; Muller, D. A. *Nature* **2011**, *469*, 389-92.

52. Tapasztó, L.; Nemes-Incze, P.; Dobrik, G.; Jae Yoo, K.; Hwang, C.; Biró, L. P. *Appl.Phys. Lett.* **2012**, *100*, 053114.

53. Geng, D.; Wu, B.; Guo, Y.; Huang, L.; Xue, Y.; Chen, J.; Yu, G.; Jiang, L.; Hu, W.; Liu, Y. *Proc. Natl. Acad. Sci.* **2012**, 1-5.

54. Wu, W.; Jauregui, L. A; Su, Z.; Liu, Z.; Bao, J.; Chen, Y. P.; Yu, Q. *Adv. Mater.* **2011**, *23*, 4898-903.

55. Yu, Q.; Jauregui, L. A; Wu, W.; Colby, R.; Tian, J.; Su, Z.; Cao, H.; Liu, Z.; Pandey, D.; Wei, D.; Chung, T. F.; Peng, P.; Guisinger, N. P.; Stach, E. A; Bao, J.; Pei, S.-S.; Chen, Y. P. *Nat. Mater.* **2011**, *10*, 443-9.

56. Yoon, T.; Shin, W. C.; Kim, T. Y.; Mun, J. H.; Kim, T.-S.; Cho, B. J. *Nano let.* **2012**, *12*, 1448-52.

57. Sun, Z.; James, D. K.; Tour, J. M. *J. Phys. Chem. Lett.* **2011**, *2*, 2425-2432..

58. Sun, Z.; Yan, Z.; Yao, J.; Beitler, E.; Zhu, Y.; Tour, J. M. *Nature* **2010**, *468*, 549-52.

59. Ji, H.; Hao, Y.; Ren, Y.; Charlton, M.; Lee, W. H.; Wu, Q.; Li, H.; Zhu, Y.; Wu, Y.; Piner, R.; Ruoff, R. S. *ACS nano* **2011**, *5*, 7656-61.

60. Byun, S.-J.; Lim, H.; Shin, G.-Y.; Han, T.-H.; Oh, S. H.; Ahn, J.-H.; Choi, H. C.; Lee, T.-W. *J. Phys. Chem. Lett.* **2011**, *2*, 493-497.

61. Yan, Z.; Peng, Z.; Sun, Z.; Yao, J.; Zhu, Y.; Liu, Z.; Ajayan, P. M. *ACS nano* **2011**, *5*, 8187-8192.

62. Perdigao L.M.A. Sabki, S. N.; Garfitt, J. M.; Capiod, P.; Beton, P. H. *J. Phys. Chem. C* **2011**, *115*, 7472-7476.

63. Shin, H. J.; Choi, W. M.; Yoon, S.-M.; Han, G. H.; Woo, Y. S.; Kim, E. S.; Chae, S. J.; Li, X.-S.; Benayad, A.; Loc, D. D.; Gunes, F.; Lee, Y. H.; Choi, J.-Y. *Adv. Mater.* **2011**, *23*, 4392-7.

64. Gadipelli, S.; Calizo, I.; Ford, J.; Cheng, G.; Hight Walker, A. R.; Yildirim, T. *J. Mater. Chem.* **2011**, *21*, 16057.

65. Microchemicals GmbH. Solvents http://www.microchemicals.eu/solvents.html (accessed May 20,2012).

66. Chavez, K. L.; Hess, D. W. *J. Electrochem. Soc.* **2001**, *148*, G640.

67. Butt, M. *J. Mater. Sci. Lett.* **1983**, *2*, 1-2.

68. Centre of micronanotechnology CMI. AZ 9200 Photoresist datasheet http://cmi.epfl.ch/photo/photo_process/files/Data_AZ9200.pdf (accessed May 23,2012).

69. Liang, X.; Sperling, B. A; Calizo, I.; Cheng, G.; Hacker, C. A.; Zhang, Q.; Obeng, Y.; Yan, K.; Peng, H.; Li, Q.; Zhu, X.; Yuan, H.; Walker, A. R. H.; Liu, Z.; Peng, L.-M.; Richter, C. A *ACS nano* **2011**, *5*, 9144-53.

70. Ferrari, a. C.; Meyer, J. C.; Scardaci, V.; Casiraghi, C.; Lazzeri, M.; Mauri, F.; Piscanec, S.; Jiang, D.; Novoselov, K. S.; Roth, S.; Geim, A. K. *Phys. Rev. Lett.* **2006**, *97*, 1-4.

71. Yu, P. Y.; Cardona, M. Fundamentals of Semiconductors, 3rd ed. ;Springer Verlag ;Berlin ,2005Hollas, J.M.; *Modern Spectroscopy*, 4th ed. ; John Wiley and Sons ;West Sussex, **2004.**

72. Malard, L. M.; Pimenta, M. A.; Dresselhaus, G.; Dresselhaus, M. S. *Phys. Rep.* **2009**, *473*, 51-87.

73. Zhang, Y.; Li, Z.; Kim, P.; Zhang, L.; Zhou, C. *ACS nano* **2012**, *6*, 126-32102.

74. Costa, S. D.; Righi, A.; Fantini, C.; Hao, Y.; Magnuson, C.; Colombo, L.; Ruoff, R. S.; Pimenta, M. A. *Solid State Commun*. **2012**, 3-6.

75. Lu, A.-Y.; Wei, S.-Y.; Wu, C.-Y.; Hernandez, Y.; Chen, T.-Y.; Liu, T.-H.; Pao, C.-W.; Chen, F.-R.; Li, L.-J.; Juang, Z.-Y. *RSC Adv*. **2012**, *2*, 3008.

76. Wang, Y.; Ni, Z.; Yu, T.; Shen, Z. X.; Wang, H.; Wu, Y.; Chen, W.; Thye, A.; Wee, S. *J. Phys.Chem. C* **2008**, 10637-10640.

77. Calizo, I.; Bao, W.; Miao, F.; Lau, C. N.; Balandin, A. A. *Appl. Phys. Lett*. **2007**, 91, 201904.

78. Lee, S.; Lee, K.; Zhong, Z. *Nano lett*. **2010,** *10*, 4702-7.

79. Lenski, D. R.; Fuhrer, M. S. *J.Appl.Phys*. 2011, *110*, 013720.

80. Ohring, M. The material science of thin films, 1st ed. ;Academic press ; London, 1992.

81. Venables, J. A.; Spiller, G. F. T.; Hanbucken, M. *Rep. Prog. Phys*. **1984**, *47*,399-459.

82. Ratsch, C.; Venables J.A.*, J. Vac. Sci. Technol*. **2003**, *21*, S96-S109.

83. Zhang, B.; Lee, W. H.; Piner, R.; Kholmanov, I.; Wu, Y.; Li, H.; Ji, H.; Ruoff, R. S. *ACS nano* **2012**, *6*, 2471-6.

84. Robinson, Z. R.; Tyagi, P.; Murray, T. M.; Ventrice, C. a.; Chen, S.; Munson, A.; Magnuson, C. W.; Ruoff, R. S. *J. Vac. Sci. Technol. A* **2012**, *30*, 011401.

85. Suk, J. W.; Kitt, A.; Magnuson, C. W.; Hao, Y.; Ahmed, S.; An, J.; Swan, A. K.; Goldberg, B. B.; Ruoff, R. S. *ACS nano* **2011,** 6916-6924.

86. Rafiee, J.; Mi, X.; Gullapalli, H.; Thomas, A. V.; Yavari, F.; Shi, Y.; Ajayan, P. M.; Koratkar, N. A *Nat. Mater*. **2012**, *11*, 217-22.

87. Ni, Z. H.; Yu, T.; Luo, Z. Q.; Wang, Y. Y.; Liu, L.; Wong, C. P.; Miao, J.; Huang, W.; Shen, Z. X. *ACS nano* **2009**, *3*, 569-574.

88. Liu, L.; Zhou, H.; Cheng, R.; Chen, Y.; Lin, Y.-C.; Qu, Y.; Bai, J.; Ivanov, I. A.; Liu, G.; Huang, Y.; Duan, X. *J. Mater. Chem*. **2012**, *22*, 1498.

89. Wu, W.; Yu, Q.; Peng, P.; Liu, Z.; Bao, J.; Pei, S.-S. *Nanotechnology* **2012**, *23*, 035603.

90. Wang, H.; Wang, G.; Bao, P.; Yang, S.; Zhu, W.; Xie, X.; Zhang, W.-Jun. *J. Am. Chem. Soc*. **2011**, 2-5.

91. Gao, L.; Ren, W.; Zhao, J.; Ma, L.-P.; Chen, Z.; Cheng, H.-M. *Appl. Phys. Lett.* **2010**, *97*, 183109.

92. Wu, B.; Geng, D.; Guo, Y.; Huang, L.; Xue, Y.; Zheng, J.; Chen, J.; Yu, G.; Liu, Y.; Jiang, L.; Hu, W. *Adv. Mater.* **2011**, *23*, 3522-5.